Journal of
Medicinal Chemistry

Article

Development of Multi-Functional Histone Deacetylase 6 Degraders with Potent Anti-Myeloma Activity

Hao Wu, Ka Yang, Zhongrui Zhang, Eric Leisten, ZIYUAN LI, Haibo Xie, Jin Liu, Kerry A. Smith, Zora Novakova, Cyril Barinka, and Weiping Tang

J. Med. Chem., **Just Accepted Manuscript** • DOI: 10.1021/acs.jmedchem.9b00516 • Publication Date (Web): 04 Jul 2019

Just Accepted

is published by the American Chemical Society. 1155 Sixteenth Street N.W., Washington, DC 20036

Development of Multi-Functional Histone Deacetylase 6 Degraders with Potent Anti-Myeloma Activity

Hao Wu[1, ‡], Ka Yang[1, ‡], Zhongrui Zhang[1,2], Eric D. Leisten[1], Ziyuan Li[1], Haibo Xie[1], Jin Liu[1], Kerry A. Smith,[1] Zora Novakova,[3] Cyril Barinka,[3] and Weiping Tang[1,2]*

[1] School of Pharmacy, University of Wisconsin-Madison, Madison, Wisconsin 53705, USA

[2] Department of Chemistry, University of Wisconsin-Madison, Madison, Wisconsin 53705, USA

[3] Institute of Biotechnology of the Czech Academy of Sciences, BIOCEV, Prumyslova 595, 252 50 Vestec, Czech Republic

Keywords: Histone Deacetylase, HDAC6, Targeted Protein Degradation, PROTAC, Multiple Myeloma

Abstract: Histone deacetylase 6 (HDAC6) primarily catalyzes the removal of acetyl group from the side chain of acetylated lysine residues in cytoplasmic proteins such as α-Tubulin and HSP90.

HDAC6 is involved in multiple disease-relevant pathways. Based on the proteolysis targeting chimera (PROTAC) strategy, we previously developed the first HDAC6 degrader by tethering a pan HDAC inhibitor with cereblon (CRBN) E3 ubiquitin ligase ligand. We herein report our new generation of multi-functional HDAC6 degraders by tethering selective HDAC6 inhibitor Next-A with CRBN ligand that can synergize with HDAC6 degradation for the anti-proliferation of multiple myeloma. This new class of degraders exhibited improved potency and selectivity for the degradation of HDAC6. After the optimization of the linker length and linking positions, we discovered potent HDAC6 degraders with nanomolar DC_{50} and promising anti-proliferation activity in multiple myeloma (MM) cells.

Introduction

Post translational modification of proteins is essential in all cellular pathways[1]. Among them, lysine acetylation is regulated by histone acetyltransferases (HATs) and histone deacetylases (HDACs). Most members of HDACs serve as epigenetic "erasers" to remove the acetyl groups of lysine residues of histone tails and promote chromatin condensation and gene suppression within the nucleus[2,3]. HDAC inhibitors can reverse this modulation by inhibiting HDAC activity and re-activate the transcription of important genes including tumor suppressors[2]. There are 11 zinc-dependent HDACs and 7 nicotinamide adenine dinucleotide (NAD^+) dependent deacetylase sirtuins (SIRTs) in the HDAC superfamily. Among them, HDAC6 is a unique member of class IIb HDACs. The cellular location of HDAC6 is in the cytoplasm rather than nuclei.[4,5] HDAC6 also has a number of non-histone substrates such as α-Tubulin[6], cortactin[7] and HSP90[5]. HDAC6 is responsible for regulating diverse cellular functions such as cell motility[7,8], immunoregulation[9,10], and aggresome formation[11,12]. Abnormal expression of HDAC6 has been observed in cancers such

as oral squamous cell carcinoma, acute myeloid leukemia, ovarian cancer, and hepatocellular carcinomas[13–16]. Selective inhibitors of HDAC6 have been developed and emerged as promising therapeutic agent for cancer treatment[13,17].

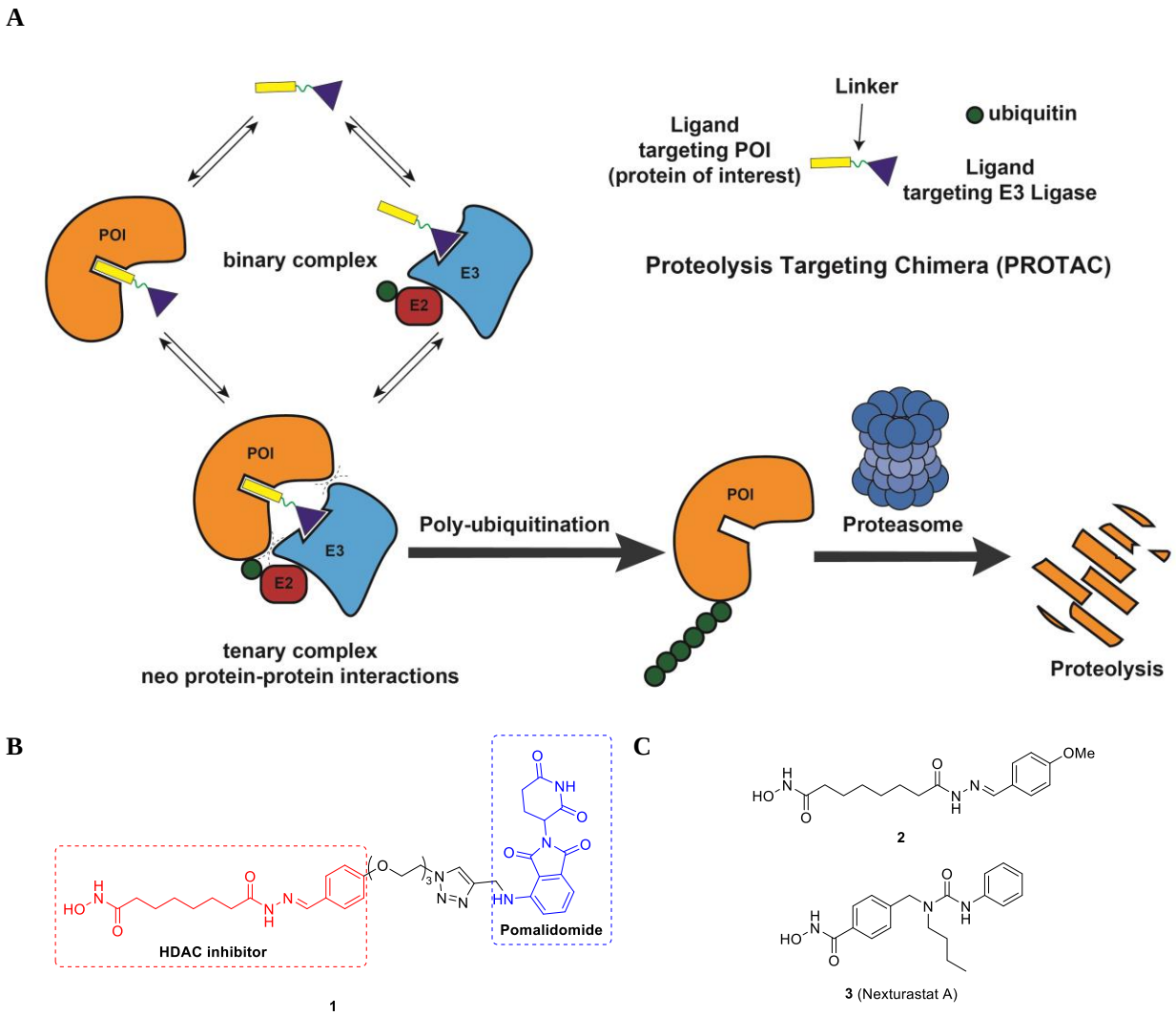

Figure 1. PROTAC strategy and HDAC6 degraders. (A) Illustration of general PROTAC induced protein ubiquitination and degradation. (B) Our previously reported HDAC6 degrader **1**. (C) "Warhead" HDAC inhibitors **2** for our previous degraders and **3** for the new degraders.

Cellular knockdown and genetic silencing of certain functional proteins are important methods in basic biological research and drug discovery. CRISPR and siRNA knockdown proteins by

changing the content of DNA or degrading mRNA. Recently, proteolysis targeting chimeras (PROTACs) emerged as a technique to induce efficient degradation of targeted protein[18] (**Figure 1A**). PROTACs are rationally designed bi-functional small molecules composed of an E3 ubiquitin ligase ligand, a ligand for the protein of interest (POI), and a linker connecting them. The chemical chimera binds to either POI or E3 ligase to form binary complex first[19]. A subsequent ternary complex formation recruits E3 ligase to be adjacent to the POI and promotes its degradation through the ubiquitination-proteasome system (UPS)[18,20,21]. To date, many disease-associated proteins have been degraded by PROTACs using three E3 ligases including cereblon (CRBN), Von Hippel-Lindau (VHL), and inhibitor of apoptosis proteins (IAPs)[22–29]. By targeting the degradation of MDM2[30] or BET[25,31,32], PROTACs exhibited excellent antitumor activity in leukemia models. These pre-clinical data underlined the significance of PROTACs in drug discovery. Furthermore, PROTACs are also useful chemical probes for target validation[26] and modulation of cellular functions[33].

The degradation of Sirt2 by PROTACs was the first published example of degraders serving as epigenetic "erasers"[27]. We previously reported degrader **1** as the first PROTAC for zinc-dependent HDACs by conjugating HDAC inhibitors with pomalidomide-linked aldehydes[34,35] (**Figure 1B**). Since there was no report on the degradation of any of these Zn-dependent HDACs prior to our studies, we used pan-HDAC inhibitor **2**[36,37] (**Figure 1C**) as the PROTAC "warhead" to examine which one of these HDACs could be degraded by PROTACs. Surprisingly, we found that compound **1** selectively degraded HDAC6 among the HDACs we examined. However, there are several limitations for these HDAC6 degraders. For example, the hydrazone linker is not hydrolytically stable and therefore not ideal for further studies. Although compound **1** selectively degrades HDAC6, other members of HDACs are still inhibited by the pan-inhibitor "warhead" as

demonstrated by the elevated level of acetylated histones. Clearly, the selectivity and potency of HDAC6 degraders need to be improved by using a completely different scaffold for further biological and pharmacological studies. A number of selective HDAC6 inhibitors have been developed in the past decade[38–44]. Among them, potent inhibitor Nexturastat A[45] (Next-A, **3**, **Figure 1C**) showed great selectivity for HDAC6 over all other HDACs. We therefore designed a new generation of selective HDAC6 degraders by attaching E3 ligase ligand pomalidomide[18,23,30,31,34] to the solvent-exposing benzene ring of HDAC6 selective inhibitor Next-A. During our investigation of the new generation HDAC6 selective degraders, Rao's group reported a class of PROTACs in 2019 by attaching a E3 ligase ligand to the alkyl chain of Next-A.[46] However, their PROTACs did not show any improved anti-proliferation activity over the parent HDAC6 inhibitor Next-A.

Despite the revolution in myeloma therapy in the last two decades, many patients are resistant to currently approved agents[47]. HDAC6 selective inhibitors have been used in combination with proteasome inhibitors[48,49], immunomodulatory drugs (IMiDs, e.g. pomalidomide and its related analogues)[50] and anti-PD-L1 antibody[51] in anti-myeloma therapeutic treatment. HDAC6 selective inhibitors showed synergy with IMiDs for the treatment of multiple myeloma in animal models and human clinical trials, though the mechanism is still not clear. Upon binding to CRBN, pomalidomide analogues are known to activate CRBN's E3 ligase activity towards ikaros family of zinc fingers (IKZFs) and promote their ubiquitination and subsequent degradation[52–54]. IKZFs become the neo-substrates of ligand-bound CRBN. The induced degradation of IKZFs by pomalidomide and its analogues are believed to be responsible for their significant anti-proliferation effect in multiple myeloma. Interestingly, PROTACs with IKZF degradation activity have also been reported in a number of cases when pomalidomide was employed as the ligand for

CRBN E3 ligase[26,55–57]. The degradation of IKZFs is often considered as undesired during the development of PROTACs. We hypothesize that multifunctional HDAC6 degraders that retain the degradation activity of IKZFs would have enhanced anti-myeloma activity. We herein report that our new generation of HDAC6 selective degraders have distinct advantages in degradation efficiency and selectivity over our previous compounds. Our new HDAC6 degraders also have significantly more potent anti-proliferation effects than the HDAC6 inhibitor Next-A in multiple myeloma cancer cell lines.

Results and Discussion

We synthesized 18 different degraders by tethering HDAC6-selective inhibitor Next-A (**3**) with CRBN E3 ligand Pomalidomide. The general synthetic route is illustrated in **Scheme 1**. Pomalidomide analogues **4a-e** containing alkyne group were synthesized by a S_NAr reaction between racemic fluoro-thalidomide (**3a** and **3b**) and aminoalkynes according to literature procedures[25]. Alkylation of *N*-Boc protected 4-aminophenol (**5**) with different α,ώ-dibromoalkanes provided intermediates **6a-e**. Subsequent nucleophilic substitution reaction with sodium azide generated compounds **7a-e** which were deprotected under boiling water or acidic conditions to give the amines **8a-e**[58]. These amines reacted with secondary amine **9** in the presence of carbonyldiimidazole (CDI) to generate urea esters **10a-e**[45]. The hydroxamic acid group was introduced to **10a-e** by utilizing hydroxylamine under basic conditions to afford hydroxamic acids **11a-e**. Finally, PROTACs **12a-r** with varying linker lengths were obtained by click reactions between azides **11a-e** and alkynes **4a-e** under typical conditions[59].

Scheme 1.[a] Synthesis of Compounds **12a-r**

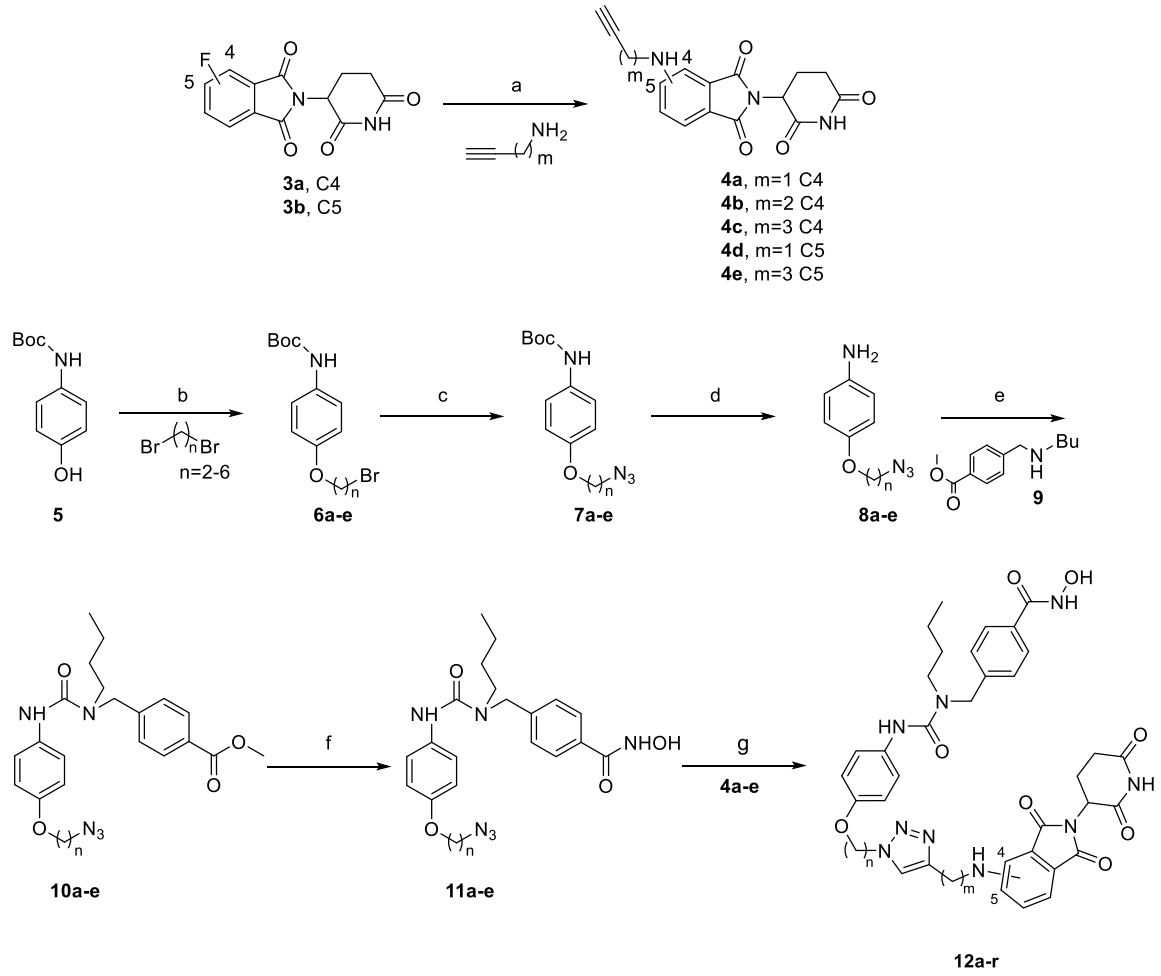

[a]Reaction conditions: (a) DIPEA, DMF, 90 °C, 17-62%; (b) K_2CO_3, MeCN, reflux, 45-70%; (c) NaN_3, DMF, 50 ºC, 66-90%; (d) H_2O, Ar reflux or TFA, DCM, 0 ºC-rt, 94-97%; (e) CDI, THF, 0 ºC-rt, 13-88%; (f) NaOH, NH_2OH/H_2O, THF, MeOH, 0 ºC-rt, 87-92%; (g) $CuSO_4$, sodium ascorbate, TBTA, H_2O/t-BuOH (1:1.5), rt, 14-80%. For compounds **3a-b** and **4a-e**, C4 means 4-substitution and C5 means 5-substitution.

These degraders are divided into to two series based on their linking position of the amino group on the phthalimide ring of Pomalidomide: C4- or C5-linked series (**Table 1**). Within each series, the degraders are different from each other by the numbers of carbon atoms between Next-A and the triazole ring (n) or between Pomalidomide and the triazole ring (m). It is known that both C-4 and C-5 positions of Pomalidomide are exposed to solvent and can be the position to place the linker for PROTACs [53,60]. The para position of the aniline in Next-A was chosen to place the linker

because it is well known that the aromatic ring "cap" of HDAC inhibitors is exposed to the solvent[61,62].

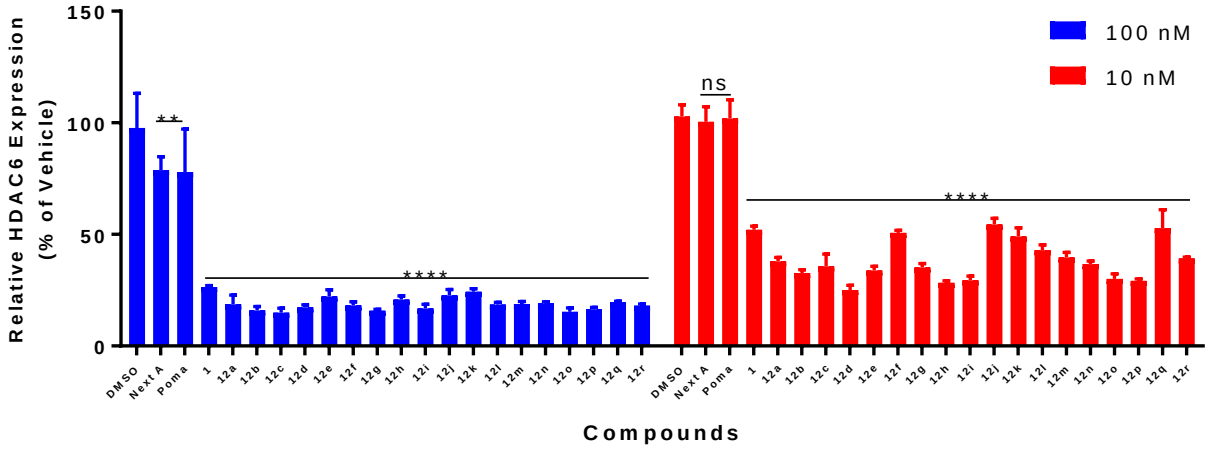

Figure 2. Screening of compounds for HDAC6 degradation activity by in-cell ELISA. MM1S cells were treated with compounds at 100 nM or 10 nM for 6 h. Data was normalized to vehicle (DMSO) treated group and bar graph represented as mean of relative HDAC6 protein level (n = 3) with ± SD as error bar. Statistical significance was analyzed by one-way ANOVA. Not significant (ns) $P > 0.05$, $^{**}P \leqslant 0.01$, $^{****}P \leqslant 0.0001$.

Table 1. Screening of compounds for HDAC6 degradation activity

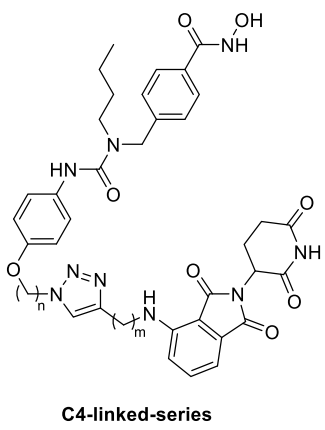

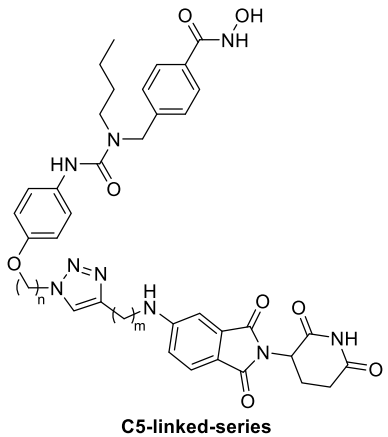

Cpd	n	m	Degradation (%)[a]		Cpd	n	m	Degradation (%)[a]	
			100 nM	10 nM				100 nM	10 nM
Next-A	N/A		21.2 ± 3.5	-0.4 ± 3.9	**-**				
Poma	N/A		22.1 ± 11.2	-2.0 ± 4.8	**-**				
1	N/A		73.5 ± 0.3	47.9 ± 0.9	**-**				
12a	2	1	81.3 ± 2.3	62.1 ± 1.0	**12l**	2	1	81.4 ± 0.6	57.1 ± 1.4
12b	3	1	84.1 ± 1.0	67.3 ± 0.8	**12m**	3	1	81.2 ± 0.6	60.3 ± 1.3
12c	4	1	85.0 ± 1.2	64.3 ± 3.2	**12n**	4	1	80.9 ± 0.4	63.3 ± 0.8
12d	5	1	82.7 ± 1.7	74.9 ± 1.2	**12o**	5	1	84.7 ± 1.0	69.9 ± 1.3
12e	6	1	77.8 ± 1.7	66.1 ± 1.1	**12p**	6	1	83.5 ± 0.5	70.8 ± 0.4
12f	2	2	81.8 ± 0.9	49.3 ± 0.6	**-**				
12g	3	2	84.2 ± 0.4	64.8 ± 1.0	**-**				
12h	4	2	79.2 ± 0.9	71.7 ± 0.5	-				
12i	2	3	83.1 ± 1.0	70.6 ± 1.1	**12q**	2	3	80.4 ± 0.3	47.2 ± 4.8
12j	3	3	77.3 ± 1.5	45.6 ± 1.6	**12r**	3	3	81.9 ± 0.4	60.9 ± 0.4
12k	4	3	75.7 ± 0.8	50.9 ± 2.2	-				

[a] Degradation percentage calculated from **Figure 2**. Degradation percentage represents [100% -mean (± SD) of HDAC6 relative expression of biological replicates (n = 3)].

To screen the new series of degraders, we first developed and validated a high throughput in-cell ELISA assay (**Supplementary Figure S1**). We treated the compounds at 100 nM and 10 nM in MM1S cells for 6 h (**Figure 2A**). Resulting cells were then fixed and analyzed by in-cell ELISA. Comparing with vehicle, Next-A and Pomalidomide didn't affect the expression of HDAC6 at 10 nM and had very minimal effects at 100 nM. At both concentrations, all degraders decreased significant amount of HDAC6 protein. The degradation level was calculated and listed in **Table 1**. Degraders including **1** at 100 nM degraded 73.5% to 85.0% of HDAC6 with minor difference.

At 10 nM concentration of compounds, obvious structure-activity-relationship (SAR) was observed. While only 47.9% of HDAC6 expression was suppressed by our previously reported degrader **1**, several new degraders are much more potent. For example, **12d**, **12h**, **12i**, **12o** and **12p** all achieved about 70% degradation. Among the C4-linked series, **12d** with medium length linker (5 + 1) achieved most degradation in sub-series **12a-e** (m = 1). For sub-series **12f-h** (m = 2), the degradation potency increased when linkers were elongated and **12h** (4 + 2) was the best. Within sub-series **12i-k** (m = 3), **12i** with the shortest linker (2 + 3) turned out to be the most potent degrader. Among C5-linked series, the potency of sub-series **12l-p** (m = 1) increased with the linker length. Compounds **12o** (5 + 1) and **12p** (6 + 1) have the similar potency for the degradation of HDAC6. Sub-series **12q-r** (m = 3) showed relative low effects for the degradation of HDAC6. The above results suggest the optimal total number of methylene units in the linker is about 6 and the C4-linked series are slightly more potent than the C5-series, which might relate to the accessibility of the degrader-recruited E3 ligase to the available ubiquitination site(s) of HDAC6. It appeared that both the distance and linking positions contributed to the degradation efficiency. We prepared and tested the C4-linked series of compounds first. After learning the optimal length of the linker, only selected C5-linked series of compounds were prepared and tested for SAR studies.

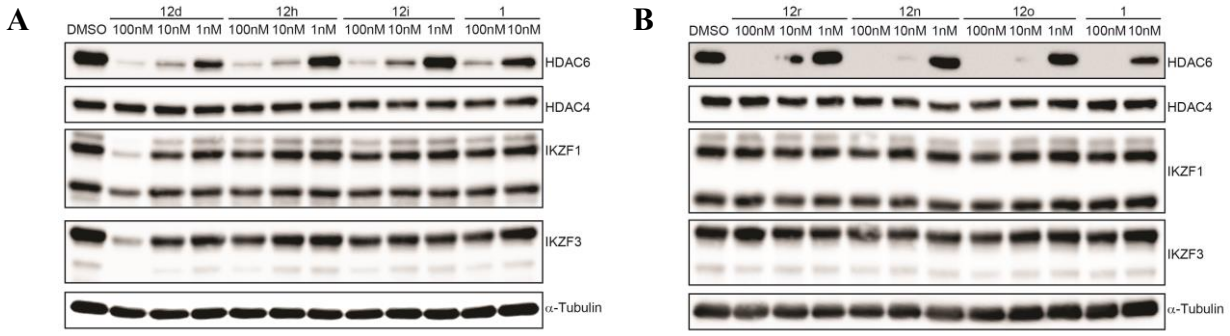

Figure 3. Western blot analysis of MM1S cells treated with selected candidates from C4-lined series (**A**) and C5-lined series (**B**) for 6 h.

After the identification of the most potent candidates from each sub-series, we incubated selected compounds at 100 nM, 10 nM and 1 nM for western blot analysis (**Figure 3**) to confirm the ELISA results. Class II HDAC4 was selected for comparison. For selected compounds from C4- or C5-linked series, all of them presented maximal effects at 100 nM and degraded significant amount of HDAC6 at 10 nM. Clearly, our previous HDAC6 degrader **1** degraded much less HDAC6 at 10 nM concentration. The results from Western blot are consistent with the screening results by ELISA.

As discussed before, pomalidomide and its analogues are known to activate CRBN's E3 ligase activity for the degradation of IKZFs. Interestingly, among the candidates we examined, only **12d** retained the induced degradation of IKZF1/3 by pomalidomide moiety at 100 nM. IKZFs regulate the expression of interferon regulatory factor 4 (IRF4) and c-Myc to affect the proliferation of multiple myeloma (MM)[52]. The downregulation of IKZF 1 and 3 by pomalidomide and its analogues are believed to be responsible for their significant anti-proliferation effect in multiple myeloma. PROTACs with IKZF degradation activity have been reported in a number of cases[26,55–57] and the IKZFs are often considered as "off-targets" during the development of these PROTACs. Our results indicate that the IKZF degradation activity can be impacted by the linker position and

the functional group next to the phthalimide ring. In our case, the triazole ring linked to C4 position likely contributed to the induced interaction between CRBN and IKZFs.

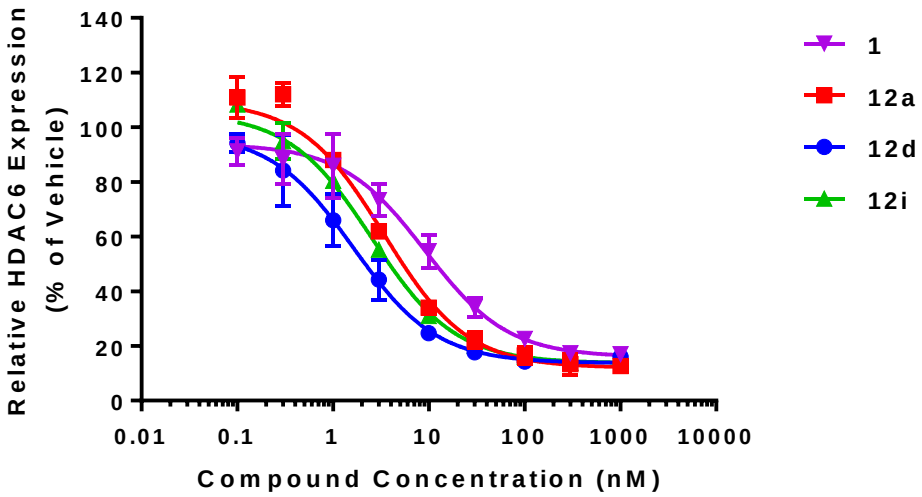

Figure 4. Dose response of selected degrader candidates. MM1S cells treated in 6 h and analyzed by in-cell ELISA. Data was normalized to vehicle (DMSO) treated group and dot plot represented as mean relative expression (n = 3) with ± SD as error bar. Nonlinear fitting of [Iinhibitor] vs. response (three parameters) was generated by GraphPad Prism with R^2 from 0.97 to 0.99.

Table 2. DC_{50}[a] and D_{max}[b] of Selected Degraders

Cpd	DC_{50} (nM)	D_{max} (Vehicle%)
1	9.12 ± 1.64	84.07 ± 2.41
12a	3.41 ± 0.52	88.01 ± 2.23
12d	1.64 ± 0.24	86.26 ± 1.70
12i	2.54 ± 0.32	86.30 ± 1.67

[a]The concentration at which half-maximal degradation was achieved. [b]The maximum

percentage of degradation. [a,b]Values with ± SD obtained from nonlinear fitted data in **Figure 4**.

To examine the potency of the selected candidates, we used in-cell ELISA to analyze the HDAC6 content in MM1S cells treated with **12a**, **12d** and **12i** and compared them with degrader **1**. We measured the amount of cellular HDAC6 in response to concentrations of compounds from 0.1 nM to 1 μM (**Figure 4**). DC_{50} and D_{max} were calculated and listed in **Table 2**. Targeted protein degradation is often attenuated at higher PROTAC concentrations, due to competitive formation of POI-PROTAC or E3 ligase-PROTAC binary complexes instead of the desired POI-PROTAC-E3 ligase ternary complex, which is termed as "hook effect".[63] All degraders achieved 84-88% maximal degradation and no "hook effect" was observed at concentrations ≤ 1 μM. Our new degraders had single-digit nanomolar DC_{50}, which was about 3 to 5 fold improvement from DC_{50} of 9.1 nM for degrader **1**. Among these degraders, **12d** showed excellent potency with a DC_{50} at around 1.6 nM. As discussed above, most PROTACs were designed to avoid degrading other proteins except the targeted POIs. However, in our study, we hypothesized that HDAC6 degraders with IKZF degradation will have enhanced anti-proliferation effect in MM1S cells. Since compound **12d** showed promising IKZF degradation activity (**Figure 3A**), we further characterized its activity and mechanism of action.

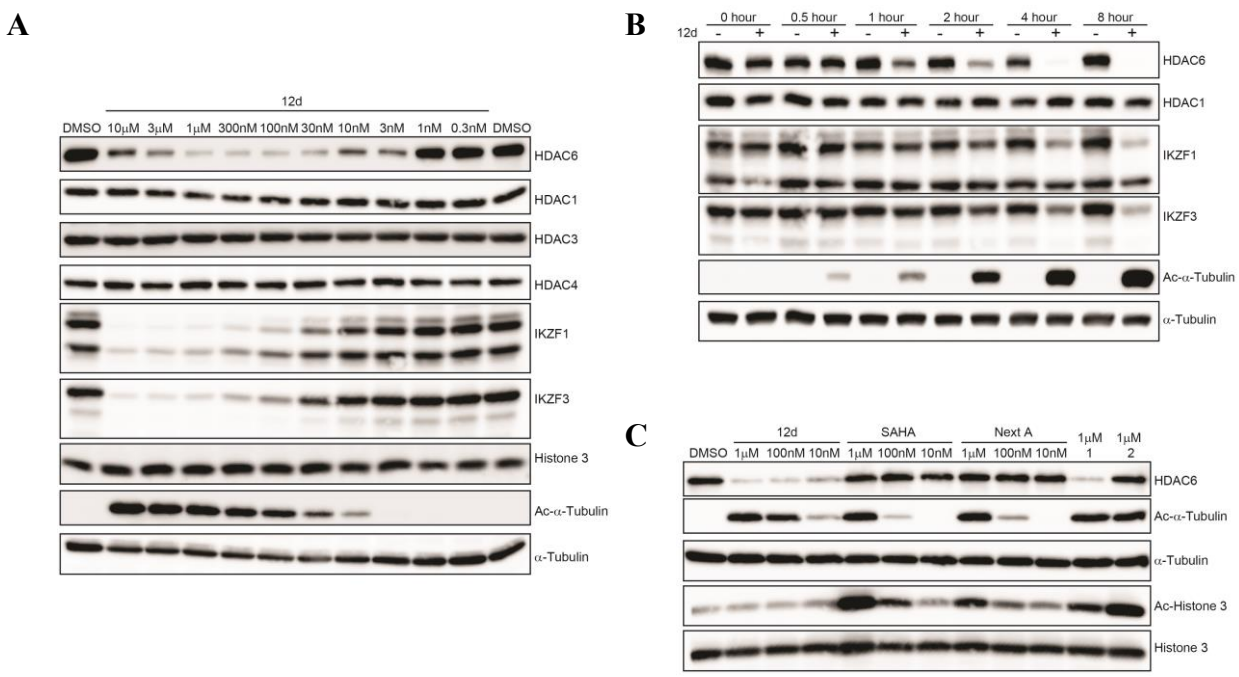

Figure 5. Degrader **12d** selectively promote HDAC6 degradation in MM1S cells. (**A**) Dose response of **12d** at concentration from 0.3 nM to 10 μM. (**B**) Time-course change of proteins expression under treatment of **12d** at 100 nM. See **Supplementary Figure S2A** and **S2B** for full blot of (**A**) and (**B**) with other loading controls. (**C**) Comparison of HDAC6 degraders and HDAC inhibitors.

To evaluate the activity and selectivity of 1**2d**, we first performed a full dose response experiment with compound concentrations ranging from 0.3 nM to 10 μM in MM1S cells (**Figure 5A**) for several representative HDACs, IKZFs, and Ac-Tubulin. The result indicated that only the expression of HDAC6 was affected among the HDACs we examined. Degrader **12d** reduced HDAC6 protein content at as low as 3 nM and achieved maximal effects around 30 nM. The "Hook effect" was observed at 3 μM or above due to formation of binary complexes[63]. The degradation of IKZFs started from 30 nM and was dose-dependent. It is interesting to see the more efficient

degradation of HDAC6, which requires the binding of both ligands to their protein targets, than that of IKZFs, which only requires the binding of Pomalidomide motif to CRBN. In addition to the distinct mechanism, the different turnover rates of HDAC6 and IKZFs may also contribute to the observed results. The acetylated Tubulin level was also dose-dependent. At higher concentrations (3 μM and 10 μM), Tubulin acetylation was not decreased in response to recovered HDAC6 expression by "hook effect". The elevated Tubulin acetylation at higher concentrations of **12d** was likely due to more significant HDAC6 inhibition because the degrader contained a potent HDAC6 inhibitor motif.

To probe the efficiency of **12d**, we treated MM1S with 100 nM **12d** and monitored the change of HDAC6 protein level by time (**Figure 5B**). The HDAC6 degradation started around 1 h and reached maximal degradation effect at 4 h. The degradation of IKZFs was only observed after 4 h. Meanwhile, HDAC1 was not affected and the acetylation of Tubulin was accumulated by time. To study the re-synthesis rate of HDAC6 after degradation, we performed "wash-out" experiment (**Supplementary Figure S2D**). Cells were treated with 100 nM **12d** for 6 h and then washed with PBS to remove remaining degraders. HDAC6 expression was monitored for 48 h. HDAC6 was not fully recovered within 48 h, suggesting the slow turnover rate of HDAC6. Interestingly, IKZF3 was quickly recovered after 12 h, indicating the fast re-synthesis rate of IKZFs, which might be one of the reasons for the requirement of higher concentrations of compounds for the degradation of IKZF. We also tested selected degraders in other cell lines (**Supplementary Figure S3**) and they are effective among all tested cancer cell lines.

To further examine the selectivity of our new generation of HDAC6 degraders, we compared compound **12d** with SAHA, Next-A, degrader **1** and pan-inhibitor **2** for the change of acetylated α-Tubulin and acetylated histone H3 (**Figure 5C**). Compound **12d** increased the acetylated

Tubulin at 100 nM while SAHA and Next-A didn't, indicating that the elevated acetylated Tubulin was primarily due to HDAC6 degradation rather than the inhibition by "warhead" Next-A. We didn't observe any increase of acetylated histone H3 by the treatment **12d**, which is in sharp contrast to the strong acetylated histone H3 signal induced by SAHA, suggesting high selectivity of the degrader. Comparing to our previously developed degrader **1**, compound **12d** also showed significantly improved selectivity for increasing the level of acetylated Tubulin over acetylated histone H3, indicating the advantage of replacing a pan-HDAC inhibitor by HDAC6 selective inhibitor as the ligand of HDAC6 for PROTACs. We also compared the activity of **12d** and Next-A in biochemical assays (**Supplementary Table S3**). Indeed, **12d** has an IC_{50} of 8.7±1.9 against HDAC6, which is similar to Next-A (IC_{50} = 3.8±2.1). Their IC_{50}s against other HDACs are in the range of 300 to >30,000 nM.

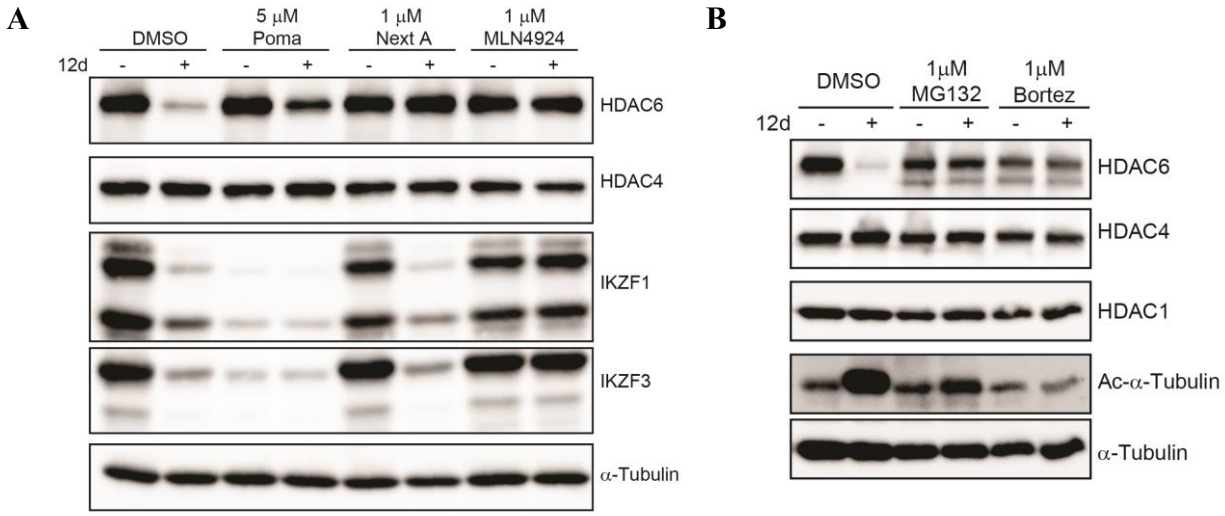

Figure 6. Mechanistic studies of compound **12d**. Western blot analysis of MM1S cells with pre-treatment of E3 ligase ligand Pomalidomide, HDAC6 inhibitor Next-A or NAE inhibitor MLN 4924 (**A**) or pre-treatment of proteasome inhibitor MG132 or Bortezomib (**B**) or vehicle

(DMSO) for 1 h and it is followed by the treatment of 100 nM **2d** or vehicle (DMSO) for 6 h. See **Supplementary Figure S2C** for full blot of (**B**) with IKZFs and Tubulin.

To support the involvement of ubiquitination-proteasome system for the decrease of HDAC6 protein level, we co-treated the degrader with binding competitors or pathway blockers (**Figure 6**). The co-treatment of degrader with Pomalidomide or Next-A recovered HDAC6 level while the degradation of IKZFs was preserved (**Figure 6A**), indicating that the binding of the degrader to both HDAC6 and CRBN E3 ligase are required for induced protein degradation. Moreover, it also confirmed the role of Pomalidomide moiety in modulating IKZFs. Neddylation of cullin RING ligase (CRL) by NEDD8-Activating Enzyme (NAE) regulated CRL's activity as E3 ligase[32,64]. Inhibiting neddylation by NAE inhibitor MLN4924 resulted in abolishing the degradation of both HDAC6 and IKZFs (**Figure 6A**). We also used proteasome inhibitor MG132 and Bortezomib to block the down-stream proteasome degradation (**Figure 6B**). Under the co-treatment of both inhibitors, no degradation of HDAC6 or of other HDACs was observed. Acetylated Tubulin level was suppressed as well. This confirms that HDAC6 degradation is responsible for the increased acetylation of its substrates rather than inhibition by the "warhead" moiety. To exclude the possible transcriptional impact by degraders, we used qRT-PCR to examine the mRNA level of HDAC6 and related genes (**Supplementary S4**). We observed little effects on HDACs and IKZFs after 6 h treatment of degrader **12d**. It is consistent with the hypothesis that the cellular knockdown of HDAC6 is due to direct protein degradation, not by transcriptional downregulation.

Scheme 2. [a] Synthetic Route to Deactivated Degraders **13** and **15**

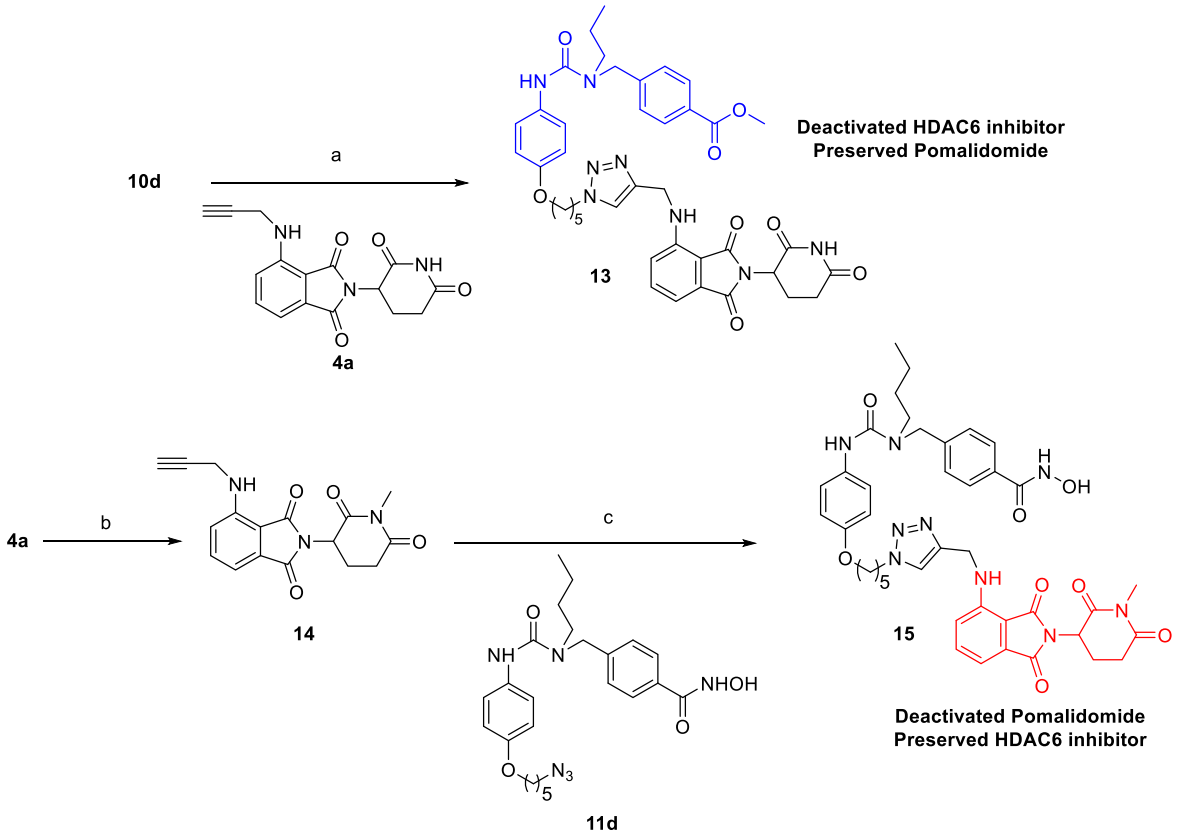

[a]Reaction conditions: (a) $CuSO_4$, sodium ascorbate, TBTA, H_2O/t-BuOH (1:1.5), rt, 93%; (b) Cs_2CO_3, CH_3I, DMF, 44%; (c) $CuSO_4$, sodium ascorbate, TBTA, H_2O/t-BuOH (1:1.5), rt, 70%.

Our HDAC6 degrader **12d** thus has three functions: inhibition of HDAC6 by the Next-A motif, degradation of IKZFs by the pomalidomide moiety, and the degradation of HDAC6 through the formation of the ternary complex. The former two functions can be achieved by the combination of HDAC6 selective inhibitor and pomalidomide. The third function is unique for HDAC6 degraders. Since HDAC6 selective inhibitors showed synergy with pomalidomide and its related analogues for the treatment of multiple myeloma in animal models and human clinical trials[50,65,66], we envision that HDAC6 degrader **12d** would have enhanced anti-myeloma activity over the combination of HDAC6 selective inhibitor and pomalidomide.

To rule out the potential cell-permeability issue, we synthesized compounds **13** and **15**, which have similar molecular weight and size comparing to **12d**, for better comparison. We blocked the binding of **13** to HDAC6 by replacing the hydroxamic acid with a methyl ester. We also blocked the binding of **15** to CRBN by attaching a methyl group to the key imide NH in **15**. Compounds **13** and **15** were synthesized according to the routes shown in **Scheme 2**. Compound **13** was synthesized using the procedure described for the synthesis of compounds **12a-r** with ester **10d** and alkyne **4a** as the starting materials. Replacing the hydroxamic acid group on Next-A by a methyl ester group was expected to prevent the binding of the resulting product to zinc co-factor of HDAC6. N-methylation of the glutarimide ring of the pomalidomide moiety in **4a** yielded compound **14,** which was converted to product **15** using click reaction. The *N*-methylated Pomalidomide moiety has been frequently used as the negative control for Pomalidomide-based PROTACs[23]. Western blot analysis proved that both compounds **13** and **15** were inactive in MM1S (**Supplementary Figure S5A**). Compound **13** induced limited HDAC6 degradation which might due to hydrolysis of carboxylic ester to carboxylic acid, which is a very weak ligand for zinc.

We performed single treatment or co-treatment as combined therapy (1 μM) for 72 hours in MM1S cells (**Figure 7A**). Next-A had minor effects on cell growth while **15** was totally inactive. Pomalidomide, **13** and degrader **1** shared similar antiproliferation effects at this concentration. We didn't observe statistically significant synergy of dual treatment with **13** + **15** (1:1) or dual treatment with Pomalidomide + Next-A (1:1) comparing with single treatment of **13** or Pomalidomide ($P > 0.05$). The dual treatment of Pomalidomide + Next-A (1:1) is slightly more potent than that of **13** + **15** (1:1). However, the single treatment of **12d** improved about 19% ($P = 0.0017$) and 11% ($P = 0.0213$) growth inhibition comparing with the combination sets of **13** + **15** (1:1) and Pomalidomide + Next-A (1:1), respectively. To further confirm the observed

enhancement, we studied the anti-proliferation in response to **12d** from 0.3 nM to 3 μM (**Figure 7B**). We compared this single treatment with dual treatment of **13** and **15** to rule out the potential complication derived from cell permeability issue. The resulting EC_{50} and maximal inhibition was listed in **Table 3**. Although the EC_{50} of **12d** (74.9 ± 11.3) appeared higher than the combination of **13**+**15** (23.5 ± 6.3) or **13** (17.7 ± 2.8) alone, it is clear that the relatively higher EC_{50} for **12d** is due to its lower bottom or the higher maximal growth inhibition. The three curves almost overlap at concentrations lower than 100 nM. At concentrations higher than 100 nM, degrader **12d** starts to inhibit the growth of the cell much more significantly than **13** alone or the combination of **13** and **15**. The maximal inhibition of **12d** (63.1 ± 1.8) is much higher than that of the combination of **13** and **15** (42.6 ± 1.9) or **13** alone (44.0 ± 1.2).

The combination of **13** and **15** failed to work synergistically, indicating that the HDAC6 degradation, other than inhibition, was crucial to the enhanced antiproliferation by degrader **12d** in MM1S cells. Hence, we concluded that the HDAC6 degradation and IKZF degradation had synergistic effects at higher concentration of the degrader. For 48 h treatment of **12d** in MM1S, we observed the cleavages of Caspase-3 and PARP in dose dependent manner (**Supplementary Figure S5B**), suggesting that the synergy was derived from degrader-promoted cell apoptosis.

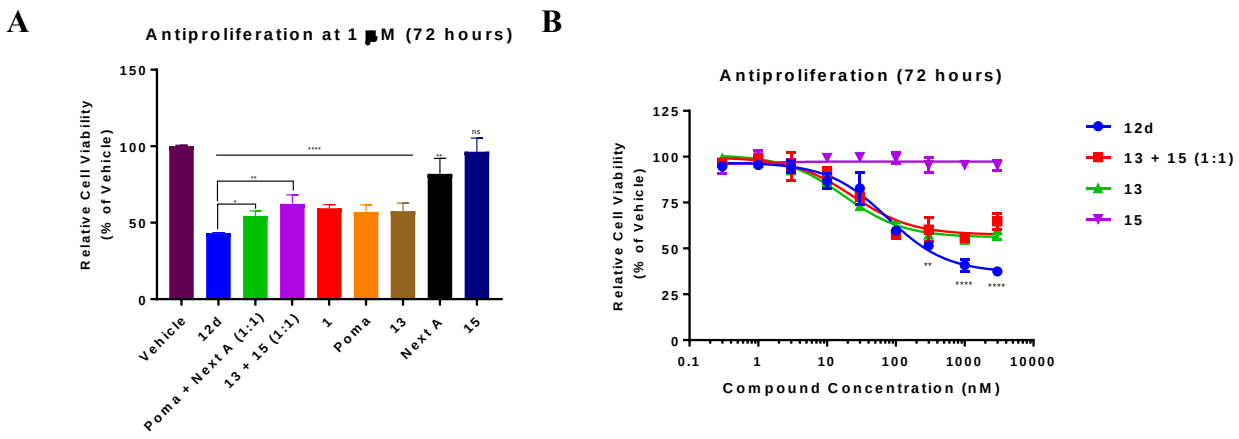

Figure 7. Antiproliferation of **12d** in multiple myeloma. (**A**) Cell viability of MM1S cells treated with compounds at 1 μM for 72 h. (**B**) Cell viability of MM1S cells treated with compounds at concentrations from 0.3 nM to 3 μM for 72 h. All data was normalized to vehicle (DMSO) treated group and dot plot represented as mean of relative viability (n = 3) with ± SD as error bar. For curve in (**B**), nonlinear fitting of [Inhibitor] vs. response (three parameters) was generated by GraphPad Prism with R^2 from 0.92 to 0.97. Statistical significance was analyzed by one-way ANOVA for (**A**) and two-way ANOVA for (**B**). See **Supplementary Table S2** for details of (**B**). Not significant (ns) $P > 0.05$, $^{*}P \leqslant 0.05$, $^{**}P \leqslant 0.01$, $^{***}P \leqslant 0.001$, $^{****}P \leqslant 0.0001$.

Table 3. EC_{50} of Antiproliferation in MM1S

	EC_{50} (nM) [a]	**Maximal Inhibition (%) [b]**
12d	74.9 ± 11.3	63.1 ± 1.8
13 + 15 (1:1)	23.5 ± 6.3	42.6 ± 1.9
13	17.7 ± 2.8	44.0 ± 1.2

[a]The concentration at which half-maximal growth inhibition was achieved. [b]The maximum percentage of

growth inhibition. [a,b]Values with ± SD obtained from nonlinear fitted data in **Figure 7B**.

CONCLUSION

In this study, we reported the development of a new generation of HDAC6 degraders by tethering Pomalidomide and HDAC6 selective inhibitor Next-A. By varying the linker length and linking positon, we discovered potent and selective HDAC6 degrader **12d** that retains the degradation activity of IKZFs. Further investigation confirmed its mechanism of action. The antiproliferation study demonstrated the advantage of our HDAC6 degraders over HDAC6 inhibitor alone, IMiD alone, or its combination, presumably because of the multi-functions of the degrader. Our results highlighted the power and utility of PROTACs as a novel strategy for the development of therapeutics against multiple myeloma.

Experimental Section

General Information in Synthetic Chemistry. All reactions were conducted under a positive pressure of dry argon in glassware that had been oven dried prior to use. Anhydrous solutions of reaction mixtures were transferred via an oven dried syringe or cannula. All solvents were dried prior to use unless noted otherwise. Thin layer chromatography (TLC) was performed using precoated silica gel plates. Flash column chromatography was performed with silica gel. ^{1}H and ^{13}C nuclear magnetic resonance spectra (NMR) were recorded on Bruker 400 MHz and 500 MHz spectrometers. ^{1}H NMR spectra were reported in parts per million (ppm) referenced to 7.26 ppm of $CDCl_3$ or referenced to the center line of a septet at 2.50 ppm of DMSO-d_6. Signal splitting patterns were described as singlet (s), doublet (d), triplet (t), quartet (q), quintet (quint), or multiplet (m), with coupling constants (*J*) in hertz. High resolution mass spectra (HRMS) were performed on an Electron Spray Injection (ESI) TOF mass spectrometer. The liquid chromatography mass

spectrometry LC-MS analysis of final products was processed on Agilent 1290 Infinity II LC system using Poroshell 120 EC-C18 column (5 cm × 2.1 mm, 1.9 μm) for chromatographic separation. Agilent 6120 Quadrupole LC/MS with multimode Electrospray Ionization plus atmospheric pressure chemical ionization (MM-ES+APCI) was used for detection. The mobile phases were 5.0% methanol and 0.1% formic acid in purified water (A) and 0.1% formic acid in methanol (B). The gradient was held at 5% (0-0.2 min), increased to 100% at 2.5 min, then held at isocratic 100% B for 0.4 min and then immediately stepped back down to 5% for 0.1 min re-equilibration. The flow rate was set at 0.8 mL/min. Column temperature was set at 40 °C. The purities of all the final compounds were determined to be over 95% by LC-MS. See Supporting Information for ^{1}H and ^{13}C NMR spectrums and LC-MS purity analysis of all compounds.

Pomalidomide analogues. Alkyne materials **4a-e** were made according to literature procedures[25,34].

2-(2,6-Dioxopiperidin-3-yl)-4-(prop-2-yn-1-ylamino)isoindoline-1,3-dione 4a (30% yield): ^{1}H NMR (500 MHz, $CDCl_3$): δ 2.12-2.16 (m, 1H), 2.27 (t, *J* = 2.3 Hz, 1H), 2.70-2.93 (m, 3H), 4.10 (dd, *J* = 6.1, 2.4 Hz, 2H), 4.92 (dd, *J*= 12.3, 5.4 Hz, 1H), 6.45 (t, *J* = 5.8 Hz, 1H), 7.03 (d, *J* = 8.5 Hz, 1H), 7.20 (d, *J* = 7.2 Hz, 1H), 7.56-7.59 (m, 1H), 7.97 (s, 1H). ^{13}C NMR (126 MHz, DMSO): δ 22.7, 31.6, 32.3, 49.0, 72.5, 79.7, 111.3, 112.2, 117.4, 132.5, 136.0, 145.5, 167.6, 169.2, 169.4, 172.3. LC−MS(ESI) *m/z* $(M + H)^+$: 312.1; calcd for $C_{16}H_{13}N_3O_4$ $(M + H)^+$: 312.1.

4-(But-3-yn-1-ylamino)-2-(2,6-dioxopiperidin-3-yl)isoindoline-1,3-dione 4b (59% yield): ^{1}H NMR (400 MHz, DMSO): δ 1.98-2.07 (m, 1H), 2.43-2.49 (m, 2H), 2.53-2.65 (m, 2H), 2.82-2.95 (m, 2H), 3.43-3.53 (m, 2H), 4.96-5.17 (m, 1H), 6.65-6.75 (m, 1H), 6.98-7.10 (m, 1H), 7.16 (d, *J* = 8.6 Hz, 1H), 7.53-7.65 (m, 1H), 11.09 (s, 1H). ^{13}C NMR (100 MHz, DMSO): δ 172.8, 170.1,

168.8, 167.3, 146.0, 136.3, 132.2, 117.3, 110.8, 109.4, 81.9, 72.9, 48.6, 40.7, 31.0, 22.1, 18.6. LC−MS(ESI) *m/z* $(M + H)^+$: 326.0; calcd for $C_{17}H_{15}N_3O_4$ $(M + H)^+$: 326.1.

2-(2,6-Dioxopiperidin-3-yl)-4-(pent-4-yn-1-ylamino)isoindoline-1,3-dione 4c (62% yield): ^{1}H NMR (400 MHz, $CDCl_3$): δ 1.84-1.92 (m, 2H), 2.09-2.16 (m, 1H), 2.30-2.38 (m, 2H), 2.68-2.99 (m, 4H), 3.40-3.49 (m, 2H), 4.96-4.83 (m, 1H) 6.23-6.35 (m, 1H), 6.98-6.88 (m, 1H) 7.20-7.04 (m, 1H), 7.47-7.55 (m, 1H), 8.12 (brs, 1H). ^{13}C NMR (100 MHz, DMSO): δ 172.8, 170.1, 167.3, 162.3, 146.3, 136.3, 132.3, 117.3, 110.5, 109.3, 83.8, 71.7, 48.5, 43.0, 41.0, 35.8, 27.5, 15.3. LC−MS(ESI) *m/z* $(M + H)^+$: 340.1; calcd for $C_{18}H_{17}N_3O_4$ $(M + H)^+$: 340.1.

2-(2,6-Dioxopiperidin-3-yl)-5-(pent-4-yn-1-ylamino)isoindoline-1,3-dione 4d (17% yield): ^{1}H NMR (400 MHz, DMSO): δ 1.99-2.02 (m, 1H), 2.53-2.60 (m, 2H), 2.83-2.93 (m, 1H), 3.19 (s, 1H), 4.07 (br, 2H), 5.03-5.06 (m, 1H), 6.94 (d, J = 8.4 Hz, 1H), 7.04 (br, 1H), 7.41-7.44 (m, 1H), 7.62 (d, J = 8.4 Hz, 1H), 11.07 (br, 1H). ^{13}C NMR (100 MHz, DMSO): δ 173.3, 170.6, 168.1, 167.6, 153.9, 134.4, 125.4, 117.9, 117.1, 106.4, 81.2, 74.3, 49.2, 32.2, 31.5, 22.7. LC−MS(ESI) *m/z* $(M + H)^+$: 312.0; calcd for $C_{16}H_{13}N_3O_4$ $(M + H)^+$: 312.1.

2-(2,6-Dioxopiperidin-3-yl)-5-(prop-2-yn-1-ylamino)isoindoline-1,3-dione 4e (20% yield): ^{1}H NMR (400 MHz, DMSO): δ 1.67-1.74 (m, 2H), 1.94-1.98 (m, 1H), 2.22-2.26 (m, 2H), 2.46 (br, 2H), 2.78-2.88 (m, 2H), 3.18-3.21 (m, 2H), 4.99 (dd, J = 5.6, 12.8 Hz, 1H), 6.81 (d, J = 8.4 Hz, 1H), 6.92 (s, 1H), 7.06-7.16 (m, 1H), 7.53 (d, J = 8.4 Hz, 1H), 11.02 (br, 1H). ^{13}C NMR (100 MHz, DMSO): δ 172.8, 170.2, 167.7, 167.1, 154.3, 134.2, 125.1, 116.1, 83.9, 71.6, 48.6, 41.3, 31.0, 27.2, 22.2, 15.4. LC−MS(ESI) *m/z* $(M + H)^+$: 340.0; calcd for $C_{18}H_{17}N_3O_4$ $(M + H)^+$: 340.1.

General Procedure for Preparing PROTACs 12a-r

A mixture of compound **5** (500 mg, 2.4 mmol), 1,2-dibromoethane (0.82 mL, 9.6 mmol) and potassium carbonate (1.3g, 9.6 mmol) in acetonitrile (5 mL) was stirred at 90℃ overnight. The

mixture was cooled to room temperature and poured into water (10 mL), then extracted with ethyl acetate (10 mL x 3). The combined organic phases were washed with brine (20 mL), dried over anhydrous sodium sulfate, and concentrated under reduced pressure. The residue was purified by silica gel flash column chromatography (eluted with 5% ethyl acetate in hexane) to afford compound **6a** (482 mg, 64%).

A suspension of compound **6a** (300 mg, 0.95 mmol) and sodium azide (308 mg, 4.7 mmol) in DMF (5 mL) was stirred at 50 ℃for 4h. Then EtOAc and water were added. The organic layer was separated and washed once with water. The resulting aqueous layer was extracted once with EtOAc. The combined organic layer was dried over with Na_2SO_4 and concentrated in vacuo. The residue was purified by silica gel chromatograph to give the product **7a** (224 mg, 85%).

For the syntheses of **8a-c (**n=2-4): In a 250 mL round bottle flask filled with 100 mL of water, **7a-c** was added. Then the flask topped with a condenser was dipped in a 110 ℃ oil bath. TLC was used to monitor the progress of the reaction. The reaction mixture was cooled down after 12h and was extracted with ethyl acetate. The extract was washed with brine, dried over with anhydrous Na_2SO_4, and then concentrated in vacuo. The residue was purified by column chromatography on silica gel with ethyl acetate/hexane (1:1, v/v) to afford the free amine **8a-c** (95-97%).

For the syntheses of **8d-e** (n=5, 6): To a solution of azide (**7d-e**) in DCM (45 ml) was added TFA (30 eq) dropwise at 0℃. The resulting mixture was stirred at room temperature for 4h. Upon completion as indicated by TLC, the reaction was quenched by aqueous $NaHCO_3$, then extracted with ethyl acetate (10 mL x 3). The combined organic layers were washed with brine (20 mL), dried over anhydrous sodium sulfate, and concentrated under reduced pressure. The residue was purified by silica gel flash column chromatography (eluted with 20% ethyl acetate in hexane) to afford compounds **8d-e** (94-96%).

A solution of **8a** (140 mg, 0.78 mmol) in THF (2 mL) was added carbonyldiimidazole (CDI: 153 mg, 0.94 mmol) at room temperature under an atmosphere of Ar, and the resulting solution was stirred for 2h. Then **9** (173 mg, 0.78 mmol) in THF (2 ml) was added dropwise to the reaction mixture and the resulting mixture was stirred overnight. The reaction was quenched with saturated aqueous sodium bicarbonate (10 mL) and extracted with DCM (3 × 10 mL). The combined organics were washed with brine (15 mL), dried over sodium sulfate, concentrated in vacuo, and purified via silica gel chromatography, affording the urea ester **10a** as a brown oil (253 mg, 76%).

NaOH (188 mg, 4.7 mmol) was dissolved in an aqueous solution of NH_2OH (50 wt %, 1 mL) at 0 ℃. Then a solution of **10a** (250 mg, 0.59 mmol) in THF/MeOH (1:1, 3 mL total) was added dropwise where the biphasic solution became homogeneous upon compete addition. The resulting solution was stirred 1h at room temperature. The reaction was quenched with AcOH (0.35 mL, 5.64 mmol). Water (10 ml) was added and the aqueous layer was extracted three times with DCM (10 mL × 3). The combined organic layers were washed with brine (15 ml), dried over sodium sulfate, concentrated in vacuo, and purified via silica gel chromatograph, affording **11a** (231 mg, 92%).

4-((3-(4-(2-Azidoethoxy)phenyl)-1-butylureido)methyl)-N-hydroxybenzamide 11a: ^{1}H NMR (400 MHz, $CDCl_3$): δ 0.85 (t, *J* = 7.2 Hz, 3H), 1.16-1.24 (m, 1H), 1.48 (br, 2H), 1.95 (brs, 1H), 3.16 (br, 2H), 3.50 (br, 2H), 4.02 (br, 2H), 4.42 (br, 2H), 6.63-6.64 (m, 3H), 6.95-7.23 (m, 4H), 7.55 (br, 2H), 8.02 (br, 2H). ^{13}C NMR (100 MHz, $CDCl_3$): δ166.1, 156.3, 154.6, 142.2, 132.7, 130.2, 127.6, 127.1, 122.9, 114.9, 67.4, 50.3, 50.1, 47.4, 30.4, 20.2, 14.0. LC−MS(ESI) *m/z* $(M + H)^+$: 427.1; calcd for $C_{21}H_{26}N_6O_4$ $(M + H)^+$: 427.2.

Following the procedures, **11b-e** with different linker lengths were obtained.

4-((3-(4-(3-Azidopropoxy)phenyl)-1-butylureido)methyl)-N-hydroxybenzamide 11b (87% yield): ^{1}H NMR (400 MHz, $CDCl_3$): δ 0.86 (t, *J* = 7.2 Hz, 3H), 1.16-1.24 (m, 1H), 1.43-1.56 (m, 2H), 1.90-2.04 (m, 3H), 3.17 (br, 2H), 3.45 (t, *J* = 7.2 Hz, 2H), 3.87-4.01 (m, 2H), 4.44 (br, 2H), 6.61-6.82 (m, 3H), 6.79-7.22 (m, 4H), 7.56 (br, 2H), 8.48 (br, 2H). ^{13}C NMR (100 MHz, $CDCl_3$): δ 166.0, 156.2, 154.5, 142.1, 132.6, 130.1, 127.5, 127.0, 122.8, 114.8, 67.3, 50.2, 50.0, 47.3, 30.3, 20.1, 13.9. LC−MS(ESI) *m/z* $(M + H)^+$: 441.1; calcd for $C_{22}H_{28}N_6O_4$ $(M + H)^+$: 441.2.

4-((3-(4-(4-Azidobutoxy)phenyl)-1-butylureido)methyl)-N-hydroxybenzamide 11c (92% yield): ^{1}H NMR (400 MHz, $CDCl_3$): δ 0.86 (t, *J* = 7.3 Hz, 3H), 1.16-1.33 (m, 2H), 1.42-1.57 (m, 2H), 1.68-1.86 (m, 4H), 1.95 (s, 1H), 3.16 (s, 2H), 3.31 (t, *J* = 6.5Hz, 2H), 3.81-3.97 (m, 2H), 4.43 (s, 2H), 6.60-6.85 (m, 3H), 6.92-7.23 (m, 4H), 7.75 (br, 1H), 8.51 (br, 2H). ^{13}C NMR (100 MHz, $CDCl_3$): δ 165.9, 156.3, 155.2, 142.1, 131.9, 130.1, 127.5, 127.0, 122.9, 114.6, 67.5, 51.2, 50.0, 47.3, 30.3, 26.5, 25.7, 20.1, 13.9. LC−MS(ESI) *m/z* $(M + H)^+$: 455.1; calcd for $C_{23}H_{30}N_6O_4$ $(M + H)^+$: 455.2.

4-((3-(4-((5-Azidopentyl)oxy)phenyl)-1-butylureido)methyl)-N-hydroxybenzamide 11d (79% yield): ^{1}H NMR (400 MHz, $CDCl_3$): δ 0.87 (t, *J* = 7.2 Hz, 3H), 1.13-1.40 (m, 2H), 1.43-1.56 (m, 4H), 1.58-1,69 (m, 2H), 1.70-1.81 (m, 2H), 3.19 (s, 2H), 3.27 (t, *J* = 6.8 Hz, 2H), 3.79-3.95 (m, 2H), 4.47 (s, 2H), 6.51-6.86 (m, 3H), 6.90-7.23 (m, 4H), 7.59 (br, 2H). ^{13}C NMR (100 MHz, $CDCl_3$): δ 165.9, 156.3, 155.4, 142.0, 131.7, 130.0, 127.5, 127.0, 122.9, 114.7, 67.9, 51.3, 50.1, 47.5, 30.3, 28.8, 28.6, 23.4, 20.1, 13.9. LC−MS(ESI) *m/z* $(M + H)^+$: 469.1; calcd for $C_{24}H_{32}N_6O_4$ $(M + H)^+$: 469.3.

4-((3-(4-((6-Azidohexyl)oxy)phenyl)-1-butylureido)methyl)-N-hydroxybenzamide 11e (90% yield): ^{1}H NMR (400 MHz, $CDCl_3$): δ 0.75-0.97 (m, 3H), 1.11-1.27 (m, 2H), 1.33-1.52 (m, 6H), 1.55-1.66 (m, 2H), 1.69-1.82 (m, 2H), 2.97-3.40 (m, 4H), 3.86 (s, 2H), 4.45 (s, 2H), 6.44-

6.80 (m, 3H), 6.89-7.22 (m, 4H), 7.61 (br, 2H). ^{13}C NMR (100 MHz, $CDCl_3$): δ 165.9, 156.3, 155.4, 142.0, 131.8, 130.1, 127.5, 127.0, 122.9, 114.7, 68.0, 51.4, 50.0, 47.4, 30.3, 29.2, 28.8, 26.5, 25.7, 20.1, 13.9.

A mixture of **11a** (20 mg, 0.05 mmol) and compound **4a** (15 mg, 0.05 mmol), tris[(1-benzyl-1H-1,2,3-triazol-4-yl)methyl]amine (5 mg, 0.001 mmol), $CuSO_4$ (1.5 mg, 0.01 mmol), sodium ascorbate (12 mg, 0.06 mmol) in *t*-BuOH:H_2O (1.5:1) (2 mL) was stirred at room temperature for 16 h. The reaction mixture was then quenched with water (5 mL) and extracted with dichloromethane (10 mL x 3). The combined organic phases were washed brine (50 mL), dried over anhydrous sodium sulfate, and concentrated under reduced pressure. The residue was purified by silica gel flash column chromatography (eluted with 30% methanol in dichloromethane) to afford the **12a** (14 mg, 40%).

4-((1-Butyl-3-(4-(2-(4-(((2-(2,6-dioxopiperidin-3-yl)-1,3-dioxoisoindolin-4-yl)amino)methyl)-1H-1,2,3-triazol-1-yl)ethoxy)phenyl)ureido)methyl)-N-hydroxybenzamide 12a (m=1, n=2, C4 position): ^{1}H NMR (400 MHz, DMSO): δ 0.70-0.90 (m, 3H), 1.22-1.32 (m, 2H), 1.33-1.56 (m, 2H), 1.91-2.14 (m, 1H), 2.52-2.70 (m, 2H), 2.79-2.95 (m, 1H), 3.36-3.58 (m, 3H), 4.12-4.86 (m, 7H), 4.96-5.17 (m, 1H), 6.51-7.43 (m, 8H), 7.47-7.79 (m, 2H), 7.87-8.64 (m, 2H), 11.10 (brs, 1H). ^{13}C NMR (100 MHz, DMSO): δ 173.3, 170.5, 169.2, 167.7, 164.4, 155.8, 153.5, 146.3, 145.0, 142.9, 136.6, 134.4, 132.6, 127.4, 123.9, 122.3, 118.1, 114.8, 111.4, 110.2, 66.9, 55.4, 49.5, 49.0, 46.5, 38.1, 31.5, 30.4, 29.5, 22.6, 19.9, 14.2. HRMS (EI) calcd. for $C_{37}H_{39}N_9O_8$ $(M + H)^+$ 738.3000, found 738.2974. Purity: >98% (LCMS).

Following the procedure for **12a**, compounds **12b-r** were prepared.

4-((1-Butyl-3-(4-(3-(4-(((2-(2,6-dioxopiperidin-3-yl)-1,3-dioxoisoindolin-4-yl)amino)methyl)-1H-1,2,3-triazol-1-yl)propoxy)phenyl)ureido)methyl)-N-hydroxybenzamide 12b (m=1, n=3, C4 position, 40% yield): ^{1}H NMR (400 MHz, DMSO): δ 0.85 (t, *J* = 7.3 Hz, 3H), 1.24-1.31 (m, 2H), 1.41-1.53 (m, 2H), 1.97-2.07 (m, 1H), 2.16-2.28 (m, 2H), 2.51-2.64 (m, 2H), 2.81-2.96 (m, 1H), 3.21-3.27 (m, 1H), 3.83-3.91 (m, 2H), 4.44-4.53 (m, 2H), 4.49 (t, *J* = 7.0 Hz, 1H), 4.57-4.62 (m, 3H), 4.98-5.13 (m, 1H), 6.78 (d, *J* = 9.0 Hz, 1H), 7.00-7.11 (m, 2H), 7.16 (d, *J* = 8.6 Hz, 1H), 7.27-7.42 (m, 4H), 7.51-7.60 (m, 1H), 7.72 (d, *J* = 8.0 Hz, 1H), 8.06 (s, 1H), 8.22 (s, 1H), 10.97-11.39 (m, 2H). ^{13}C NMR (100 MHz, DMSO): δ 172.8, 170.1, 168.8, 167.3, 164.1, 155.5, 153.6, 145.8, 144.5, 142.5, 136.2, 133.7, 132.1, 131.4, 127.0, 123.0, 122.0, 117.6, 114.2, 110.9, 109.7, 105.4, 64.6, 49.0, 48.6, 46.6, 46.1, 37.7, 31.0, 30.0, 29.6, 22.2, 19.5, 13.8.HRMS (EI) calcd. for $C_{38}H_{41}N_9O_8$ $(M + H)^+$ 752.3156, found 752.3160. Purity: 98% (LCMS).

4-((1-Butyl-3-(4-(4-(4-(((2-(2,6-dioxopiperidin-3-yl)-1,3-dioxoisoindolin-4-yl)amino)methyl)-1H-1,2,3-triazol-1-yl)butoxy)phenyl)ureido)methyl)-N-hydroxybenzamide 12c (m=1, n=4, C4 position, 45% yield): ^{1}H NMR (400 MHz, DMSO): δ 0.85 (br, 3H), 1.14-1.22 (m, 1H), 1.34-1.72 (m, 4H), 1.78-2.04 (m, 3H), 2.52-2.66 (m, 2H), 2.81-2.96 (m, 1H), 3.39-3.47 (m, 1H), 3.83-3.94 (m, 2H), 4.13-4.28 (m, 2H), 4.32-4.44 (m, 2H), 4.53-4.67 (m, 3H), 5.01-5.15 (m, 1H), 6.69-6.88 (m, 2H), 7.00-7.21 (m, 3H), 7.24-7.44 (m, 4H), 7.52-7.64 (m, 1H), 7.66-7.77 (m, 1H), 8.05 (br, 1H), 8.21 (br, 1H), 10.98-11.32 (m, 2H). ^{13}C NMR (100 MHz, DMSO): δ 172.8, 170.1, 168.8, 167.3, 155.5, 153.8, 145.8, 136.1, 133.4, 132.1, 128.8, 127.0, 122.9, 122.0, 117.6, 114.1, 110.9, 109.7, 66.9, 49.0, 46.1, 37.7, 31.0, 30.7, 30.0, 26.6, 25.8, 22.2, 22.2, 19.5, 13.8. HRMS (EI) calcd. for $C_{39}H_{43}N_9O_8$ $(M + H)^+$ 766.3313, found 766.3309. Purity: 96% (LCMS).

4-((1-Butyl-3-(4-((5-(4-(((2-(2,6-dioxopiperidin-3-yl)-1,3-dioxoisoindolin-4-yl)amino)methyl)-1H-1,2,3-triazol-1-yl)pentyl)oxy)phenyl)ureido)methyl)-N-hydroxybenzamide 12d (m=1, n=5, C4 position, 83% yield): ^{1}H NMR (400 MHz, DMSO): δ 0.61 (brs, 3H), 0.91-1.28 (m, 6H), 1.34-1.48 (m, 2H), 1.52-1.67 (m, 2H), 1.71-1.87 (m, 1H), 2.21-2.27 (m, 2H), 2.52-2.76 (m, 1H), 3.01-3.25 (m, 3H), 3.49-3.68 (m, 2H), 3.94-4.17 (m, 2H), 4.21-4.50 (m, 3H), 4.67-4.98 (m, 1H), 6.37-6.63 (m, 2H), 6.69-7.18 (m, 6H), 7.20-8.06 (m, 4H), 10.66-11.08 (m, 1H). ^{13}C NMR (100 MHz, DMSO): δ 172.8, 170.1, 168.8, 167.3, 155.5, 153.9, 145.9, 144.4, 136.1, 133.4, 132.1, 127.0, 122.8, 122.1, 117.6, 114.1, 110.9, 109.7, 67.3, 49.3, 49.0, 48.6, 46.1, 37.7, 31.0, 30.0, 29.5, 28.1, 22.6, 22.2, 19.5, 13.8. HRMS (EI) calcd. for $C_{40}H_{45}N_9O_8$ $(M + H)^+$ 780.3469, found 780.3464. Purity: >98% (LCMS).

4-((1-Butyl-3-(4-((6-(4-(((2-(2,6-dioxopiperidin-3-yl)-1,3-dioxoisoindolin-4-yl)amino)methyl)-1H-1,2,3-triazol-1-yl)hexyl)oxy)phenyl)ureido)methyl)-N-hydroxybenzamide 12e (m=1, n=6, C4 position, 75% yield): ^{1}H NMR (400 MHz, DMSO): δ 0.71-0.98 (m, 3H), 1.11-1.52 (m, 8H), 1.56-1.88 (m, 4H), 1.95-2.16 (m, 1H), 2.52-2.67 (m, 2H), 2.80-3.00 (m, 1H), 3.23-3.47 (m, 3H), 3.75-3.97 (m, 2H), 4.23-4.44 (m, 2H), 4.49-4.84 (m, 3H), 4.92-5.19 (m, 1H), 6.57-6.91 (m, 2H), 6.92-7.43 (m, 6H), 7.47-8.31 (m, 3H), 10.88-11.35 (m, 1H). ^{13}C NMR (100 MHz, DMSO): δ 172.8, 170.1, 168.8, 167.3, 155.5, 154.0, 145.8, 144.4, 136.1, 133.3, 132.1, 127.0, 122.7, 122.1, 117.6, 114.0, 110.9, 109.7, 67.4, 49.3, 49.0, 48.6, 46.1, 37.7, 31.0, 30.0, 29.6, 28.6, 25.6, 24.9, 22.2, 19.5, 13.8. HRMS (EI) calcd. for $C_{41}H_{47}N_9O_8$ $(M + H)^+$ 794.3626, found 794.3686. Purity >98% (LCMS).

4-((1-Butyl-3-(4-(2-(4-(2-((2-(2,6-dioxopiperidin-3-yl)-1,3-dioxoisoindolin-4-yl)amino)ethyl)-1H-1,2,3-triazol-1-yl)ethoxy)phenyl)ureido)methyl)-N-hydroxybenzamide 12f (m=2, n=2, C4 position, 47% yield): ^{1}H NMR (400 MHz, DMSO): δ 0.71-0.88 (m, 3H), 1.19-

1.32 (m, 2H), 1.33-1.47 (m, 2H), 1.80-2.11 (m, 2H), 2.53-2.67 (m, 2H), 2.82-2.99 (m, 3H), 3.54-3.67 (m, 2H), 3.84-4.77 (m, 7H), 4.89-5.17 (m, 1H), 6.61-7.40 (m, 8H), 7.47-7.82 (m, 2H), 7.86-8.44 (m, 2H), 11.10 (br, 1H). ^{13}C NMR (100 MHz, DMSO): δ 172.8, 170.1, 168.8, 167.3, 155.3, 153.1, 146.1, 144.1, 136.3, 134.0, 132.2, 127.0, 123.1, 121.9, 117.2, 114.4, 110.6, 109.3, 66.5, 54.9, 49.0, 46.0, 41.7, 31.0, 29.9, 28.2, 25.1, 22.2, 19.4, 13.8. HRMS (EI) calcd. for $C_{38}H_{41}N_9O_8$ $(M + H)^+$ 752.3156, found 752.3121. Purity: >98% (LCMS).

4-((1-Butyl-3-(4-(3-(4-(2-((2-(2,6-dioxopiperidin-3-yl)-1,3-dioxoisoindolin-4-yl)amino)ethyl)-1H-1,2,3-triazol-1-yl)propoxy)phenyl)ureido)methyl)-N-hydroxybenzamide

12g (m=2, n=3, C4 position, 17% yield): ^{1}H NMR (400 MHz, DMSO): δ 0.86 (t, *J* = 7.4 Hz, 3H), 1.25-1.33 (m, 2H), 1.36-1.40 (m, 1H), 1.43-1.55 (m, 2H), 1.98-2.07 (m, 1H), 2.14-2.26 (m, 2H), 2.53-2.63 (m, 2H), 2.81-3.00 (m, 3H), 3.49-3.65 (m, 3H), 3.84-3.97 (m, 2H), 4.35-4.74 (m, 4H), 5.05 (dd, *J* = 12.8, 5.0 Hz, 1H), 6.67-6.74 (m, 1H), 6.75-6.87 (m, 2H), 7.03 (d, *J* = 7.0 Hz, 1H), 7.12 (d, *J* = 8.5 Hz, 1H), 7.26-7.40 (m, 3H), 7.58 (t, *J* = 7.9 Hz, 1H), 7.72 (d, *J* = 7.8 Hz, 1H), 7.99 (s, 1H), 8.22 (s, 1H), 11.10 (m, 1H). ^{13}C NMR (100 MHz, DMSO): δ 173.8, 170.0, 168.8, 167.3, 155.5, 153.6, 146.1, 144.0, 142.4, 136.3, 133.7, 132.2, 127.0, 122.7, 121.8, 117.2, 114.2, 110.6, 109.3, 64.6, 54.9, 49.0, 46.4, 46.1, 41.7, 31.0, 30.0, 29.6, 25.1, 22.2, 19.5, 13.8. HRMS (EI) calcd. for $C_{39}H_{43}N_9O_8$ $(M + H)^+$ 766.3313, found 766.3276. Purity: >98% (LCMS).

4-((1-Butyl-3-(4-(4-(4-(2-((2-(2,6-dioxopiperidin-3-yl)-1,3-dioxoisoindolin-4-yl)amino)ethyl)-1H-1,2,3-triazol-1-yl)butoxy)phenyl)ureido)methyl)-N-hydroxybenzamide

12h (m=2, n=4, C4 position, 55% yield): ^{1}H NMR (400 MHz, DMSO): δ 0.79-0.87 (m, 3H), 1.23-1.31 (m, 2H), 1.40-1.52 (m, 2H), 1.57-1.67 (m, 2H), 1.85-2.13 (m, 4H), 2.54-2.63 (m, 2H), 2.84-2.99 (m, 3H), 3.45-3.66 (m, 3H), 3.81-3.95 (m, 2H), 4.27-4.46 (m, 2H), 4.50-4.67 (m, 2H), 4.97-5.10 (m, 1H), 6.67-6.85 (m, 3H), 6.97-7.15 (m, 2H), 7.27-7.34 (m, 3H), 7.53-7.63 (m, 1H), 7.69-

7.74 (m, 1H), 7.89-8.01 (m, 1H), 8.21 (br, 1H), 10.95-11.59 (m, 1H). ^{13}C NMR (100 MHz, DMSO): δ 172.8, 170.1, 168.8, 167.3, 155.5, 153.8, 146.2, 144.0, 142.5, 136.3, 133.5, 132.2, 131.4, 127.0, 122.5, 122.0, 117.2, 114.1, 110.6, 109.3, 66.9, 54.9, 49.0, 46.1, 41.7, 31.0, 30.0, 27.8, 26.6, 25.7, 25.1, 22.2, 19.5, 13.8. HRMS (EI) calcd. for $C_{40}H_{45}N_9O_8$ $(M + H)^+$ 780.3469, found 780.3444. Purity: 95% (LCMS).

4-((1-Butyl-3-(4-(2-(4-(3-((2-(2,6-dioxopiperidin-3-yl)-1,3-dioxoisoindolin-4-yl)amino)propyl)-1H-1,2,3-triazol-1-yl)ethoxy)phenyl)ureido)methyl)-N-hydroxybenzamide 12i (m=3, n=2, C4 position, 47% yield): ^{1}H NMR (400 MHz, DMSO): δ 0.77-0.93 (m, 3H), 1.02-1.19 (m, 2H), 1.33-1.55 (m, 2H), 1.79-2.12 (m, 4H), 2.52-2.65 (m, 2H), 2.67-2.94 (m, 3H), 3.39-3.57 (m, 2H), 3.92-4.74 (m, 7H), 4.97-5.17 (m, 1H), 6.55-6.88 (m, 3H), 6.95-7.16 (m, 2H), 7.19-7.41 (m, 3H), 7.51-7.76 (m, 2H), 7.91-8.27 (m, 2H), 11.05-11.22 (m, 1H). ^{13}C NMR (100 MHz, DMSO): δ 172.8, 170.1, 168.9, 167.3, 155.4, 153.1, 146.3, 136.3, 134.0, 132.2, 127.0, 122.5, 121.9, 117.2, 114.4, 110.4, 109.2, 69.8, 66.5, 49.0, 48.6, 46.0, 41.3, 31.0, 30.0, 28.4, 22.4, 22.2, 19.4, 13.8. HRMS (EI) calcd. for $C_{39}H_{43}N_9O_8$ $(M + H)^+$ 766.3313, found 766.3284. Purity: >98% (LCMS).

4-((1-Butyl-3-(4-(3-(4-(3-((2-(2,6-dioxopiperidin-3-yl)-1,3-dioxoisoindolin-4-yl)amino)propyl)-1H-1,2,3-triazol-1-yl)propoxy)phenyl)ureido)methyl)-N-hydroxybenzamide 12j (m=3, n=3, C4 position, 68% yield): ^{1}H NMR (400 MHz, DMSO): δ 0.69-0.91 (m, 3H), 0.99-1.21 (m, 2H), 1.30-1.63 (m, 2H), 1.72-2.41 (m, 6H), 2.52-2.65 (m, 2H), 2.68-2.98 (m, 3H), 3.42-3.63 (m, 2H), 3.66-3.84 (m, 7H), 4.91-5.16 (m, 1H), 6.52-6.93 (m, 3H), 6.97-7.41 (m, 4H), 7.47-7.84 (m, 2H), 7.88-8.41 (m, 2H). 11.13 (br, 1H). ^{13}C NMR (100 MHz, DMSO): δ 172.8, 170.1, 168.9, 167.3, 155.4, 153.6, 146.4, 136.2, 133.6, 132.2, 122.0, 117.2,

114.1, 110.4, 109.1, 64.6, 46.4, 46.0, 41.3, 31.0, 29.9, 29.6, 28.4, 22.4, 22.2, 19.4, 13.8. HRMS (EI) calcd. for $C_{40}H_{45}N_9O_8$ $(M + H)^+$ 780.3469, found 780.3461. Purity 97% (LCMS).

4-((1-Butyl-3-(4-(4-(4-(3-((2-(2,6-dioxopiperidin-3-yl)-1,3-dioxoisoindolin-4-yl)amino)propyl)-1H-1,2,3-triazol-1-yl)butoxy)phenyl)ureido)methyl)-N-hydroxybenzamide 12k (m=3, n=4, C4 position, 37% yield): ^{1}H NMR (400 MHz, DMSO): δ 0.75-0.89 (m, 3H), 1.24-1.37 (m, 2H), 1.38-1.52 (m, 2H), 1.59-1.69 (m, 2H), 1.75-2.08 (m, 6H), 2.53-2.64 (m, 2H), 2.65-2.77 (m, 2H), 2.83-2.94 (m, 1H), 3.51-3.66 (m, 2H), 3.82-4.08 (m, 3H), 4.28-4.68 (m, 4H), 4.98-5.14 (m, 1H), 6.57-6.91 (m, 3H), 6.96-7.16 (m, 2H), 7.28-7.41 (m, 3H), 7.53-7.76 (m, 2H), 7.87-8.03 (m, 1H), 8.09-8.34 (m, 1H). ^{13}C NMR (100 MHz, DMSO): δ 172.8, 170.1, 168.9, 167.3, 155.5, 153.8, 146.4, 146.2, 136.3, 133.5, 132.2, 128.7, 127.0, 122.0, 121.9, 117.2, 114.1, 110.4, 109.1, 66.9, 49.0, 46.0, 41.3, 39.5, 31.0, 30.0, 28.4, 26.6, 25.8, 22.4, 22.2, 19.5, 13.8. HRMS (EI) calcd. for $C_{41}H_{47}N_9O_8$ $(M + H)^+$ 794.3626, found 794.3582. Purity >98% (LCMS).

4-((1-Butyl-3-(4-(2-(4-(((2-(2,6-dioxopiperidin-3-yl)-1,3-dioxoisoindolin-5-yl)amino)methyl)-1H-1,2,3-triazol-1-yl)ethoxy)phenyl)ureido)methyl)-N-hydroxybenzamide 12l (m=1, n=2, C5 position, 30% yield): ^{1}H NMR (400 MHz, DMSO): δ 0.85 (t, *J* = 6.8 Hz, 3H), 1.12-1.33 (m, 2H), 1.39-1.53 (m, 2H), 1.96-2.07 (m, 1H), 2.54-2.64 (m, 2H), 2.80-2.95 (m, 1H), 3.18-3.27 (m, 2H), 4.32 (br, 2H), 4.49 (br, 2H), 4.59 (br, 2H), 4.72 (br, 2H), 4.99-5.08 (m, 1H), 6.78 (d, *J* = 8 Hz, 2H), 6.96 (d, *J* = 7.6 Hz, 1H), 7.08 (br, 1H), 7.22-7.41 (m, 4H), 7.58 (d, *J* = 8 Hz, 2H), 7.72 (d, *J* =7.2 Hz, 2H), 8.09 (s, 1H), 8.24, (s, 1H), 9.01 (br, 1H), 11.01-11.25 (m, 2H). ^{13}C NMR (100 MHz, DMSO): δ 172.8, 170.2, 167.6, 167.2, 164.1, 155.4, 154.0, 153.0, 144.3, 142.4, 134.1, 131.4, 127.0, 125.0, 123.6, 121.9, 116.7, 114.4, 66.5, 63.1, 49.1,

46.1, 38.0, 31.0, 30.0, 22.2, 19.5, 13.8. HRMS (EI) calcd. for $C_{37}H_{39}N_9O_8$ $(M + H)^+$ 738.3000, found 738.2969. Purity: 96% (LCMS).

4-((1-Butyl-3-(4-(3-(4-(((2-(2,6-dioxopiperidin-3-yl)-1,3-dioxoisoindolin-5-yl)amino)methyl)-1H-1,2,3-triazol-1-yl)propoxy)phenyl)ureido)methyl)-N-hydroxybenzamide 12m (m=1, n=3, C5 position, 35% yield): ^{1}H NMR (400 MHz, DMSO): δ 0.85 (br, 3H), 1.06-1.16 (m, 1H), 1.39-1.59 (m, 2H), 1.98 (br, 1H), 2.23 (br, 2H), 2.50-2.66 (m, 2H), 2.78-2.96 (m, 1H), 3.19-3.35 (m, 2H), 3.90 (br, 2H), 4.33-4.69 (m, 6H), 4.92-5.13 (m, 1H), 6.79 (br, 2H), 6.95 (br, 1H), 7.07 (br, 1H), 7.33 (br, 4H), 7.58 (br, 2H), 7.73 (br, 2H), 8.08 (s, 1H), 8.25 (s, 1H), 9.00 (br, 1H), 10.86-11.30 (m, 2H). ^{13}C NMR (100 MHz, DMSO): δ 172.8, 170.2, 167.6, 167.2, 155.5, 154.0, 153.6, 144.3, 142.5, 134.1, 133.7, 131.4, 128.7, 127.7, 127.0, 125.0, 123.1, 122.0, 116.7, 114.2, 64.6, 63.1, 49.0, 46.6, 46.1, 38.1, 31.0, 30.0, 29.6, 22.2, 19.5, 13.8. HRMS (EI) calcd. for $C_{38}H_{41}N_9O_8$ $(M + H)^+$ 752.3165, found 752.3113. Purity >98% (LCMS).

4-((1-Butyl-3-(4-(4-(4-(((2-(2,6-dioxopiperidin-3-yl)-1,3-dioxoisoindolin-4-yl)amino)methyl)-1H-1,2,3-triazol-1-yl)butoxy)phenyl)ureido)methyl)-N-hydroxybenzamide 12n (m=1, n=4, C5 position, 49% yield): ^{1}H NMR (400 MHz, DMSO): δ 0.81 (t, *J* = 7.2 Hz, 3H), 1.15-1.19 (m, 2H), 1.37-1.48 (m, 2H), 1.54-1.67 (m, 2H), 1.84-1.93 (m, 2H), 2.40-2.48 (m, 2H), 2.76-2.93 (m, 1H), 3.21-3.30 (m, 2H), 3.82-3.91 (m, 2H), 4.31-4.39 (m, 2H), 4.40-4.49 (m, 2H), 4.57 (br, 2H), 4.93-5.09 (m, 1H), 6.75 (d, *J* = 8.8 Hz, 2H), 6.93 (d, *J* = 8.0 Hz, 1H), 7.04 (br, 1H), 7.26-7.32 (m, 5H), 7.53 (d, *J* = 8.4 Hz, 1H), 7.61-7.67 (m, 1H), 7.70 (d, *J* = 8 Hz, 2H), 8.03 (s, 1H), 8.26 (s, 1H), 11.03-11.36 (m, 2H). ^{13}C NMR (100 MHz, DMSO): δ 172.8, 170.2, 167.7, 167.2, 155.5, 154.1, 153.8, 144.2, 142.5, 134.1, 133.5, 131.4, 128.7, 127.8, 127.0, 127.0, 125.0, 123.0, 122.1, 116.6, 114.1, 66.9, 63.1, 55.0, 49.1, 46.1, 38.1, 31.0, 30.0, 26.7,

25.8, 22.3, 19.5, 13.8. HRMS (EI) calcd. for $C_{39}H_{43}N_9O_8$ $(M + H)^+$ 766.3313, found 766.3310. Purity: 96% (LCMS).

4-((1-Butyl-3-(4-((5-(4-(((2-(2,6-dioxopiperidin-3-yl)-1,3-dioxoisoindolin-5-yl)amino)methyl)-1H-1,2,3-triazol-1-yl)pentyl)oxy)phenyl)ureido)methyl)-N-hydroxybenzamide 12o (m=1, n=5, C5 position, 43% yield): ^{1}H NMR (400 MHz, DMSO): δ 0.82-0.88 (m, 3H), 1.14-1.23 (m, 2H), 1.31-1.40 (m, 2H), 1.43-1.51 (m, 2H), 1.62-1.74 (m, 2H), 1.79-1.91 (m, 2H), 1.92-2.04 (m, 1H), 2.52-2.61 (m, 2H), 2.76-2.96 (m, 1H), 3.47-3.72 (m, 2H), 3.78-3.92 (m, 2H), 4.35 (br, 2H), 4.47 (br, 2H), 4.59 (br, 2H), 4.96-5.09 (m, 1H), 6.75-6.81 (m, 2H), 6.91-6.98 (m, 1H), 7.02-7.13 (m, 2H), 7.21-7.44 (m, 4H), 7.49-7.61 (m, 1H), 7.66-7.76 (m, 1H), 8.04 (s, 1H), 8.22 (s, 1H), 8.99 (br, 1H), 10.94-11.36 (m, 2H). ^{13}C NMR (100 MHz, DMSO): 172.8, 170.1, 167.6, 167.1, 164.1, 156.3, 155.5, 154.0, 153.9, 144.1, 142.5, 134.0, 133.4, 131.4, 128.8, 127.4, 127.0, 125.0, 122.9, 122.1, 116.7, 114.0, 113.9, 67.3, 63.1, 49.3, 49.0, 46.1, 38.1, 31.0, 30.0, 29.5, 28.1, 22.6, 22.2, 19.5, 13.8. HRMS (EI) calcd. for $C_{40}H_{45}N_9O_8$ $(M + H)^+$ 780.3469, found 780.3470. Purity: 95% (LCMS).

4-((1-Butyl-3-(4-((6-(4-(((2-(2,6-dioxopiperidin-3-yl)-1,3-dioxoisoindolin-5-yl)amino)methyl)-1H-1,2,3-triazol-1-yl)hexyl)oxy)phenyl)ureido)methyl)-N-hydroxybenzamide 12p (m=1, n=6, C5 position, 37% yield): ^{1}H NMR (400 MHz, DMSO): 0.79-0.90 (m, 3H), 1.18-1.30 (m, 4H), 1.34-1.51 (m, 4H), 1.58-1.70 (m, 2H), 1.73-1.88 (m, 2H), 1.92-2.04 (m, 1H), 2.53-2.62 (m, 2H), 2.78-2.93 (m, 1H), 2.38-2.54 (m, 2H), 3.79-3.94 (m, 2H), 4.30-4.38 (m, 2H), 4.42-4.49 (m, 2H), 4.54-4.66 (m, 2H), 4.97-5.09 (m, 1H), 6.74-6.84 (m, 2H), 6.90-6.99 (m, 1H), 7.06 (br, 1H), 7.25-7.43 (m, 4H), 7.53-7.61 (m, 2H), 7.68-7.78 (m, 2H), 8.03 (s, 1H), 8.20 (s, 1H), 10.99-11.32 (m, 2H). ^{13}C NMR (100 MHz, DMSO): δ 172.8, 170.1, 167.6, 167.1, 164.1, 155.5, 154.0, 154.0, 144.1, 142.5, 134.0, 133.3, 131.4, 128.7, 127.7, 127.0, 125.0, 122.9,

122.1, 116.7, 114.1, 67.4, 49.3, 49.0, 48.7, 46.1, 38.1, 31.0, 30.0, 29.7, 28.6, 25.6, 24.9, 22.2, 19.5, 13.8. HRMS (EI) calcd. for $C_{41}H_{47}N_9O_8$ $(M + H)^+$ 794.3626, found 794.3582. Purity: 95% (LCMS).

4-((1-Butyl-3-(4-(2-(4-(3-((2-(2,6-dioxopiperidin-3-yl)-1,3-dioxoisoindolin-5-yl)amino)propyl)-1H-1,2,3-triazol-1-yl)ethoxy)phenyl)ureido)methyl)-N-hydroxybenzamide 12q (m=3, n=2, C5 position, 16% yield): ^{1}H NMR (400 MHz, DMSO): δ 0.84 (t, *J* = 7.2 Hz, 3H), 1.08-1.17 (m, 2H), 1.38-1.51 (m, 2H), 1.53-1.57 (m, 1H), 1.84-2.04 (m, 2H), 2.69-2.77 (m, 2H), 2.82-2.91 (m, 1H), 3.22-3.36 (m, 4H), 3.92-4.03 (m, 1H), 4.12-4.18 (m, 1H), 4.27-4.36 (m, 2H), 4.30-4.50 (m, 1H), 4.54-4.62 (m, 2H), 4.65-4.73 (m, 2H), 4.99-5.07 (m, 1H), 6.76-6.85 (m, 3H), 6.97 (br, 1H), 7.07 (br, 1H), 7.30 (d, *J* = 7.6 Hz, 1H), 7.35 (d, *J* = 7.6 Hz, 1H), 7.55 (d, *J* = 8.4 Hz, 1H), 7.73 (d, *J* = 7.6 Hz, 1H), 7.96 (s, 1H), 8.33 (s, 1H), 9.04 (br, 1H), 11.06 (br, 1H), 11.24 (br, 1H). ^{13}C NMR (100 MHz, DMSO): δ 172.8, 170.2, 167.7, 167.2, 156.3, 155.4, 154.5, 153.0, 146.3, 142.7, 142.4, 134.2, 134.1, 131.4, 127.4, 127.0, 125.1, 122.5, 121.9, 115.8, 114.4, 114.3, 113.9, 66.5, 63.0, 55.3, 49.0, 46.1, 45.3, 41.9, 31.0, 30.0, 28.0, 22.5, 19.5, 13.8. HRMS (EI) calcd. for $C_{39}H_{43}N_9O_8$ $(M + H)^+$ 766.3313, found 766.3275. Purity: 96% (LCMS).

4-((1-Butyl-3-(4-(3-(4-(3-((2-(2,6-dioxopiperidin-3-yl)-1,3-dioxoisoindolin-5-yl)amino)propyl)-1H-1,2,3-triazol-1-yl)propoxy)phenyl)ureido)methyl)-N-hydroxybenzamide 12r (m=3, n=3, C5 position, 24% yield): ^{1}H NMR (400 MHz, DMSO): δ 0.79-0.89 (m, 3H), 1.23-1.31 (m, 2H), 1.39-1.52 (m, 2H), 1.83-2.06 (m, 3H), 2.16-2.30 (m, 2H), 2.66-2.78 (m, 1H), 2.81-2.96 (m, 1H), 2.96-3.06 (m, 4H), 3.22 (br, 1H), 3.35 (br, 1H), 3.47-3.64 (m, 1H), 3.90 (br, 2H), 4.47 (br, 2H), 4.60 (br, 2H), 5.02 (br, 1H), 6.73-6.89 (m, 3H), 6.92-7.09 (m, 1H), 7.24-7.41 (m, 5H), 7.47-7.60 (m, 1H), 7.72 (br, 2H), 7.93 (s, 1H), 8.30 (s, 1H), 10.47-11.35 (m, 2H). ^{13}C NMR (100 MHz, DMSO): δ 172.8, 170.2, 167.7, 167.2, 164.0, 155.5, 154.5,

153.6, 146.3, 142.5, 134.2, 133.7, 131.4, 127.0, 127.0, 125.1, 122.1, 122.0, 115.8, 114.2, 64.6, 63.1, 49.0, 46.4, 46.1, 45.3, 31.0, 30.0, 29.6, 28.0, 22.6, 22.3, 19.5, 13.8.HRMS (EI) calcd. for $C_{40}H_{45}N_9O_8$ $(M + H)^+$ 780.3469, found 780.3426. Purity: 95% (LCMS).

Following the procedure to prepare **12a-r**, compound **13** was obtained by the same method in 93% yield.

Methyl 4-((1-butyl-3-(4-((5-(4-(((2-(2,6-dioxopiperidin-3-yl)-1,3-dioxoisoindolin-4-yl)amino)methyl)-1H-1,2,3-triazol-1-yl)pentyl)oxy)phenyl)ureido)methyl)benzoate 13: ^{1}H NMR (400 MHz, DMSO-d_6): δ 0.86 (t, *J* = 7.3 Hz, 3H), 1.14-1.21 (m, 1H), 1.24-1.30 (m, 3H), 1.31-1.39 (m, 2H), 1.42-1.54 (m, 2H), 1.63-1.75 (m, 2H), 1.80-1.91 (m, 2H), 2.00-2.08 (m, 1H), 2.55-2.64 (m, 1H), 2.82-2.95 (m, 1H), 3.29 (t, *J* = 7.6 Hz, 2H), 3.63 (s, 1H), 3.84 (s, 1H), 3.86-3.89 (m, 1H), 4.35 (t, *J* = 7.0 Hz, 2H), 4.58-4.65 (m, 4H), 5.07 (dd, *J* = 12.9, 5.4 Hz, 1H), 5.60 (s, 1H), 6.72-6.85 (m, 2H), 7.02-7.11 (m, 2H), 7.16 (d, *J* = 8.6 Hz, 1H), 7.27-7.35 (m, 2H), 7.40 (d, *J* = 8.1 Hz, 2H), 7.56 (dd, *J* = 8.5, 7.1 Hz, 1H), 7.94 (d, *J* = 8.1 Hz, 2H), 8.03 (s, 1H), 8.24 (s, 1H), 11.11 (s, 1H). ^{13}C NMR (100 MHz, DMSO): δ 172.8, 170.1, 168.8, 167.3, 166.1, 155.5, 153.9, 145.8, 145.0, 144.4, 143.7, 136.1, 133.3, 132.1, 129.3, 128.7, 128.2, 127.7, 127.3, 122.8, 122.1, 117.6, 114.0, 110.9, 109.7, 67.3, 52.7, 52.0, 49.3, 46.9, 46.2, 37.7, 31.0, 30.0, 29.5, 28.1, 22.6, 22.2, 19.5, 13.8. HRMS (EI) calcd. for $C_{41}H_{46}N_8O_8$ $(M + H)^+$ 779.3517, found 779.3475. Purity: >98% (LCMS).

To a solution of **4a** (60 mg, 0.16 mmol) in DMF (2 ml) was added Cs_2CO_3 (80 mg, 0.24 mmol) and CH_3I (15 μL, 0.24 mmol) at room temperature. The resulting mixture was stirred overnight. Upon completion as evidenced by TLC, the reaction was quenched by H_2O, then extracted with ethyl acetate (10 mL x 3). The combined organic layers were washed with brine (20 mL), dried over anhydrous sodium sulfate, and concentrated under reduced pressure. The residue was purified

by silica gel flash column chromatography (eluted with 25% ethyl acetate in hexane) to afford compound **14** (44%).

2-(1-Methyl-2,6-dioxopiperidin-3-yl)-4-(prop-2-yn-1-yl)isoindoline-1,3-dione 14: ^{1}H NMR (400 MHz, $CDCl_3$): δ 2.05-2.16 (m, 1H), 2.24-2.33 (m, 1H), 2.68-2.82 (m, 2H), 2.88-3.03 (m, 1H), 3.20 (s, 3H), 4.08 (dd, *J* = 6.1, 2.5 Hz, 2H), 4.86-4.98 (m, 1H), 6.44 (t, *J* = 6.0 Hz, 1H), 7.01 (d, *J* = 8.5 Hz, 1H), 7.18 (d, *J* = 7.1 Hz, 1H), 7.52-7.60 (m, 1H). ^{13}C NMR (100 MHz, $CDCl_3$): δ 171.4, 169.5, 169.0, 167.7, 145.6, 136.2, 132.6, 117.2, 112.8, 111.6, 79.3, 72.3, 49.8, 32.4, 32.0, 27.4, 22.2. LC−MS(ESI) *m/z* $(M + H)^+$: 326.1; calcd for $C_{17}H_{16}N_6O_4$ $(M + H)^+$: 326.1.

Following the procedure to prepare **12a-s**, compound **15** was obtained by the same method in 70% yield.

4-((1-Butyl-3-(4-((5-(4-(((2-(1-methyl-2,6-dioxopiperidin-3-yl)-1,3-dioxoisoindolin-4-yl)amino)methyl)-1H-1,2,3-triazol-1-yl)pentyl)oxy)phenyl)ureido)methyl)-N-hydroxybenzamide 15: ^{1}H NMR (400 MHz, DMSO-d_6): δ 0.66-0.96 (m, 3H), 1.28-1.52 (m, 6H), 1.62-1.76 (m, 2H), 1.77-1.92 (m, 2H), 1.97-2.11 (m, 1H), 2.51-2.63 (m, 2H), 2.69-3.83 (m, 1H), 3.02 (s, 3H), 3.14-3.34 (m, 2H), 3.71-4.00 (m, 2H), 4.21-4.41 (m, 2H), 4.46-4.81 (m, 3H), 5.01-5.28 (m, 1H), 6.57-6.94 (m, 2H), 6.98-8.32 (m, 10H). ^{13}C NMR (100 MHz, DMSO): δ 171.8, 169.8, 168.7, 167.2, 155.4, 153.9, 145.9, 144.4, 136.1, 133.3, 132.1, 128.7, 127.7, 122.8, 122.0, 117.7, 114.0, 110.9, 109.7, 67.3, 49.2, 49.1, 37.7, 31.1, 29.9, 29.5, 28.1, 26.6, 22.6, 21.4, 19.4, 13.8. HRMS (EI) calcd. for $C_{41}H_{47}N_9O_8$ $(M + H)^+$ 794.3626, found 794.3593. Purity: 98% (LCMS).

Chemical Reagents for Biology and Antibodies. Janus Green B (201677) and Resazurin sodium salt (R7017) were purchased from Sigma-Aldrich. Pomalidomide (S1567), Thalidomide (S1193), Lenalidomide (S1029), MG132 (S2619), Bortezomib (S1013) were purchased from

Selleckchem**.** SAHA (10009929) was purchased from Cayman Chemical. Antibodies against HDACs, IKZF1, IKZF3, Ac-α-Tubulin (K40), Histone-3, Ac-Histone-3 (K9), Caspase-3, PARP and anti-mouse- and anti-rabbit HRP-linked antibodies were purchased from Cell Signaling Technology (CST). Antibodies against α-Tubulin and β-Actin were purchased from R&D system.

Cell Lines and Culture Methods. Cell lines were purchased from American Type Culture Collection (ATCC) unless otherwise noted. Hela and HepG2 cells were cultured in DMEM medium (Corning, 1g/L glucose) supplemented with 10% FBS and 1% Penicillin/Streptomycin. A375, A431 and MCF-7 cells were cultured in DMEM medium (Corning, 4.5g/L glucose) supplemented with 10% FBS and 1% Penicillin/Streptomycin. MM1S, RPMI8226, A375, RS4;11 and Jurkat cells were cultured in RPMI-1640 medium (Corning) supplemented with 10% FBS, 1% Sodium Pyruvate, and 1% Penicillin/Streptomycin, 10mM HEPES. All cell lines were grown at 37°C in a humidified 5% CO_2 atmosphere.

In-cell ELISA Assay. MM1S cells were harvested and plated with $5x10^5$ cells in 100μL media per well 96-wells plate. After overnight seeding, 25 μL media containing 5X dosing concentration of the compounds or vehicle was added to each well. After 6-hour treatment at 37°C in a humidified 5% CO_2 atmosphere, cells were fixed by adding 125 μL 8% formaldehyde in TBS buffer (137 mM NaCl, 25 mM Tris, 2.7 mM potassium chloride, pH 7.6). and incubated at room temperature (RT) for 15 minutes. Removal of fixing solution was followed by one rinse and two washes with TBS-T washing buffer (137 mM NaCl, 20 mM Tris, 0.1% Tween, pH 7.6). Cells were then permeabilized by adding 100 μL 0.1% Triton-X in TBS and incubated at RT for 15 minutes. Removal of permeabilizing solution was followed by one rinse and one wash with TBS-T. Cellular endogenous peroxidases were quenched by adding 100 μL 1% H_2O_2 in TBS and incubation at RT for 20 minutes. Removal of quenching solution was followed by one rinse and one-wash with TBS-

T. Non-specific binding sites were blocked by adding 200 μL 5% BSA in TBS-T (with 0.02% NaN_3) and incubation at 4 °C overnight. Removal of blocking solution was followed by adding 50 μL primary antibody solution (HDAC6 Rabbit mAb, CST #7558, 1:1000 in 5% BSA in TBS-T with 0.02% NaN_3) and incubation at RT for 2 hours. Two or more wells treated with DMSO or untreated were added blocking solution without antibody as background control. Removal of primary antibody solution was followed by one rinse and three washes with TBS-T. Secondary antibody solution (Anti-rabbit IgG, HRP-linked Antibody, CST #7074, 1:2000 in 1% BSA in TBS-T) was added into cells and incubated at RT for 1 hour. Removal of secondary antibody solution was followed by one rinse and four washes with TBS-T. TMB substrates (BioLegend #421101) were premixed, added into cells and incubated in dark at RT for 20 minutes. Stop solution (2N H_2SO_4 in ddH_2O) was added into reaction mixture and incubated at RT for 5 minutes with gentle shaking. The optical density (OD) of each well was read at 450 nm and 570 nm by FLUOstar Omega microplate reader (BMG LABTECH). ELISA OD = OD_{450} - OD_{570}. Normalization of ELISA OD to cell number was processed by Janus Green Stain[67]. The normalized signal (NS) was calculated by followed formula:

$$NS = \frac{ELISA\ OD\ of\ sample - ELISA\ OD\ of\ background\ control}{Janus\ Green\ OD}$$

The relative HDAC6 expression was calculated by divide NS of compound treated well by average NS of vehicle/DMSO treated wells and marked as "relative HDAC6 expression % of vehicle".

Immunoblot. When the cells reached 90% confluence, they were harvested and plated $1x10^6$ cells per well in 6-well plate. After overnight seeding, the cells were treated with a solution of compounds or vehicle in culture medium. The culture medium was removed after treatment and then washed twice with cold PBS. To obtain whole cell lysate, all cells were treated with RIPA

lysis buffer (25mM Tris, pH 7-8, 150 mM NaCl, 0.1% SDS, 0.5% sodium deoxycholate, 1% Triton X-100, protease inhibitor cocktail (Roche, 1 tablet per 10 mL) and 1mM PMSF) on ice for 10 minutes. Supernatant was collected after spinning down at 16,000g at 4 °C for 15 minutes. Protein concentration was measured by using the Pierce BCA protein assay (Thermo Fisher Scientific). About 10-40 μg of total protein was mixed with 4X Laemmli Loading Dye (250 mM Tris, pH 6.8, 40% glycerol, 5% SDS, 0.005% bromophenol blue, 4% BME) and heated at 95-100°C for 5 minutes. The heated sample was then subjected to 7.5-12% SDS-PAGE and transferred to PVDF membrane (Bio-Rad). The membrane was blocked in 5% non-fat milk (Bio-rad) in TBS-T washing buffer (137 mM NaCl, 20 mM Tris, 0.1% Tween) and then incubated with primary antibodies at 4 °C overnight. The membrane was washed 3 times with TBS-T, incubated with secondary horseradish peroxidase (HRP) linked antibodies for 1 hour, then washed 3 more times with TBS-T. Clarity ECL substrate (Bio-rad) was incubated with membrane for 5 minutes. The Immunoblot was generated by ChemiDoc MP Imaging Systems (Bio-rad) and analyzed by Image J software. A band intensity bar graph was generated, and the curve was fitted using "log(inhibitor) vs. response (three parameters)" by GraphPad Prism.

Cell Viability Assay. MM1S cells were harvested and plated with $1x10^5$ cells in 100 μL media per well in 96-well plate. After overnight seeding, 25 μL media containing 5X dosing concentration of the compounds or vehicle was added to each well. After 72-hour treatment at 37°C in a humidified 5% CO_2 atmosphere, 12.5 μL 10X resazurin solution (1 mg/mL) was added to each well. Then cells were incubated at 37°C overnight. The optical density was read at 570 nm and 600 nm by platereader.

The relative viability (RV) was measured by followed formula:

$$RV = \frac{117216 \times OD_{570}\ of\ sample\ - 80586 \times OD_{600}\ of\ sample}{117216 \times OD_{570}\ of\ vehicle\ - 80586 \times OD_{600}\ of\ vehicle}$$

The bar graph was generated and by GraphPad Prism.

Real-Time Quantitative Reverse Transcription PCR. After treatment, cells were harvested and washed with cold PBS twice. Total RNA was extracted by GeneJET RNA Purification Kit (Thermo Scientific, K0731) following manufacture protocol. The concentration of RNA was measured by Plate Reader. Total RNA at normalized concentration was subjected to reverse transcription to generate cDNA library by High-Capacity cDNA Reverse Transcription Kit (Applied Biosystems, 4368814). 10 ng cDNA was mixed with primer sets and PowerUP SYBR Green Master Mix (Applied Biosystems, A25780) in 96-well optical PCR plate. Real-time PCR and fluorescent signal were processed by QuantStudio 7 Flex Real-Time PCR System. Fast cycling mode (50 °C, 2 minutes, hold; 95 °C, 2 minutes, hold; 95 °C, 1 second, then, 60 °C, 30 seconds, 40 cycles) was performed and followed with melt curve stage (1.6 °C/second to 95°C, 15 seconds; 1.6 °C/second to 60°C, 1 minute; 0.15 °C/second to 95°C, 15 seconds). C_t value at automatically selected threshold was reported and calculated by $2^{-\Delta\Delta Ct}$ method.[68] The bar graph was generated and by GraphPad Prism.

Statistical Analysis. All statistical analysis was done by GraphPad Prism. Statistical significance was analyzed by performing one-way or two-way ANOVA analysis of variance. Multiple group comparisons with vehicle or compound-treated group were followed Dunnett correction. Not significant (ns) $P > 0.05$, $^{*}P \leq 0.05$, $^{**}P \leq 0.01$, $^{**}P \leq 0.001$, $^{**}P \leq 0.0001$.

ASSOCIATED CONTENT

The Supporting Information is available free of charge on the ACS Publications website at DOI:

List of primers for qRT-PCR; statistical significance of Figure 7B; validation of in-cell ELISA; full western blots of figure 5A, 5B and 6B and “wash-out” experiment; additional western blots

analysis of proteins in A431, RPMI-8226, Jurkat, HepG2, RS4;11, A375, MCF-7 cell lines treated with 12d or 12n; qRT-PCR assays with 12d; western blots of deactivated degrader 13 and 15, and apoptosis assay with 12d; ^{1}H and ^{13}C NMR spectrums of compounds 4a-e, 11a-e, 12a-r,13, 14 and 15; LC-MS spectrums of 12a-r, 13 and 15.

Molecular string files for all of the final target compounds (CSV)

AUTHOR INFORMATION

Corresponding Author

* weiping.tang@wisc.edu

Author Contributions

‡These authors contributed equally. HW designed and synthesized all compounds. KY designed and completed most biochemical and cell-based assays.

ACKNOWLEDGMENT

We thank University of Wisconsin-Madison for the financial support. This study made use of the Medicinal Chemistry Center at UW-Madison instrumentation, funded by the UW School of Pharmacy and the Wisconsin Alumni Research Foundation (WARF). ZN and CB's work on obtaining the IC_{50}s of compounds **12d** and Next-A against a panel of HDACs was in part supported by the Czech Science Foundation (grant No 15-19640S), the CAS (RVO: 86652036) and the project "BIOCEV" (CZ.1.05/1.1.00/02.0109) from the ERDF. ZN and CB would like to thank B. Havlinova and P. Baranova for excellent technical assistance.

ABBREVIATIONS

PROTAC, proteolysis targeting chimera; IAP, Inhibitor of Apoptosis Protein; CRBN, Cereblon; VHL, Von Hippel–Lindau tumor suppressor; Cpd, Compound; SAHA, Suberoylanilide

Hydroxamic Acid (Vorinostat); Poma, Pomalidomide; ELISA, Enzyme-linked Immunosorbent Assay; PARP, poly ADP ribose polymerase; SD, Standard Deviation.

References

(1) van Kasteren, S. I.; Kramer, H. B.; Jensen, H. H.; Campbell, S. J.; Kirkpatrick, J.; Oldham, N. J.; Anthony, D. C.; Davis, B. G. Expanding the Diversity of Chemical Protein Modification Allows Post-Translational Mimicry. *Nature* **2007**, *446* (7139), 1105–1109.

(2) Falkenberg, K. J.; Johnstone, R. W. Histone Deacetylases and Their Inhibitors in Cancer, Neurological Diseases and Immune Disorders. *Nat. Rev. Drug Discov.* **2014**, *13* (9), 673–691.

(3) Johnstone, R. W. Histone-Deacetylase Inhibitors: Novel Drugs for the Treatment of Cancer. *Nat. Rev. Drug Discov.* **2002**, *1* (4), 287–299.

(4) Grozinger, C. M.; Hassig, C. a; Schreiber, S. L. Three Proteins Define a Class of Human Histone Deacetylases Related to Yeast Hda1p. *Proc. Natl. Acad. Sci. U. S. A.* **1999**, *96* (9), 4868–4873.

(5) Boyault, C.; Sadoul, K.; Pabion, M.; Khochbin, S. HDAC6, at the Crossroads between Cytoskeleton and Cell Signaling by Acetylation and Ubiquitination. *Oncogene* **2007**, *26* (37), 5468–5476.

(6) Hubbert, C.; Guardiola, A.; Shao, R.; Kawaguchi, Y.; Ito, A.; Nixon, A.; Yoshida, M.; Wang, X.-F.; Yao, T.-P. HDAC6 Is a Microtubule-Associated Deacetylase. *Nature* **2002**, *417* (6887), 455–458.

(7) Zhang, X.; Yuan, Z.; Zhang, Y.; Yong, S.; Salas-Burgos, A.; Koomen, J.; Olashaw, N.; Parsons, J. T.; Yang, X. J.; Dent, S. R.; Yao, T. P.; Lane, W. S.; Seto, E. HDAC6 Modulates Cell Motility by Altering the Acetylation Level of Cortactin SI. *Mol. Cell* **2007**, *27* (2), 197–

213.

(8) Wu, Y.; Song, S. W.; Sun, J.; Bruner, J. M.; Fuller, G. N.; Zhang, W. IIp45 Inhibits Cell Migration through Inhibition of HDAC6. *J. Biol. Chem.* **2010**, *285* (6), 3554–3560.

(9) Keremu, A.; Aimaiti, A.; Liang, Z.; Zou, X. Role of the HDAC6/STAT3 Pathway in Regulating PD-L1 Expression in Osteosarcoma Cell Lines. *Cancer Chemother. Pharmacol.* **2019**, *83* (2), 255–264.

(10) Lienlaf, M.; Perez-Villarroel, P.; Knox, T.; Pabon, M.; Sahakian, E.; Powers, J.; Woan, K. V.; Lee, C.; Cheng, F.; Deng, S.; Smalley, K. S. M.; Montecino, M.; Kozikowski, A.; Pinilla-Ibarz, J.; Sarnaik, A.; Seto, E.; Weber, J.; Sotomayor, E. M.; Villagra, A. Essential Role of HDAC6 in the Regulation of PD-L1 in Melanoma. *Mol. Oncol.* **2016**, *10* (5), 735–750.

(11) Hideshima, T.; Bradner, J. E.; Wong, J.; Chauhan, D.; Richardson, P.; Schreiber, S. L.; Anderson, K. C. Small-Molecule Inhibition of Proteasome and Aggresome Function Induces Synergistic Antitumor Activity in Multiple Myeloma. *Proc. Natl. Acad. Sci. U. S. A.* **2005**, *102* (24), 8567–8572.

(12) Kawaguchi, Y.; Kovacs, J. J.; McLaurin, A.; Vance, J. M.; Ito, A.; Yao, T.-P. The Deacetylase HDAC6 Regulates Aggresome Formation and Cell Viability in Response to Misfolded Protein Stress. *Cell* **2003**, *115* (6), 727–738.

(13) Kalin, J. H.; Bergman, J. A. Development and Therapeutic Implications of Selective Histone Deacetylase 6 Inhibitors. *J. Med. Chem.* **2013**, *56* (16), 6297–6313.

(14) Kanno, K.; Kanno, S.; Nitta, H.; Uesugi, N.; Sugai, T.; Masuda, T.; Wakabayashi, G.;

Maesawa, C. Overexpression of Histone Deacetylase 6 Contributes to Accelerated Migration and Invasion Activity of Hepatocellular Carcinoma Cells. *Oncol. Rep.* **2012**, *28* (3), 867–873.

(15) Bradbury, C. A.; Khanim, F. L.; Hayden, R.; Bunce, C. M.; White, D. A.; Drayson, M. T.; Craddock, C.; Turner, B. M. Histone Deacetylases in Acute Myeloid Leukaemia Show a Distinctive Pattern of Expression That Changes Selectively in Response to Deacetylase Inhibitors. *Leukemia* **2005**, *19* (10), 1751–1759.

(16) Bazzaro, M.; Lin, Z.; Santillan, A.; Lee, M. K.; Wang, M. C.; Chan, K. C.; Bristow, R. E.; Mazitschek, R.; Bradner, J.; Roden, R. B. S. Ubiquitin Proteasome System Stress Underlies Synergistic Killing of Ovarian Cancer Cells by Bortezomib and a Novel HDAC6 Inhibitor. *Clin. Cancer Res.* **2008**, *14* (22), 7340–7347.

(17) Wang, X.-X.; Wan, R.-Z.; Liu, Z.-P. Recent Advances in the Discovery of Potent and Selective HDAC6 Inhibitors. *Eur. J. Med. Chem.* **2018**, *143*, 1406–1418.

(18) Lai, A. C.; Crews, C. M. Induced Protein Degradation: An Emerging Drug Discovery Paradigm. *Nat. Rev. Drug Discov.* **2017**, *16* (2), 101–114.

(19) Gadd, M. S.; Testa, A.; Lucas, X.; Chan, K.; Chen, W.; Lamont, D. J.; Zengerle, M.; Ciulli, A. Structural Basis of PROTAC Cooperative Recognition for Selective Protein Degradation. *Nat. Chem. Biol.* **2017**, *13* (5), 514–521.

(20) Buckley, D. L.; Crews, C. M. Small-Molecule Control of Intracellular Protein Levels through Modulation of the Ubiquitin Proteasome System. *Angew. Chem. Int. Ed.* **2014**, *53* (9), 2312–2330.

(21) Ottis, P.; Crews, C. M. Proteolysis-Targeting Chimeras: Induced Protein Degradation as a Therapeutic Strategy. *ACS Chem. Biol.* **2017**, *12* (4), 892–898.

(22) Demizu, Y.; Okuhira, K.; Motoi, H.; Ohno, A.; Shoda, T.; Fukuhara, K.; Okuda, H.; Naito, M.; Kurihara, M. Design and Synthesis of Estrogen Receptor Degradation Inducer Based on a Protein Knockdown Strategy. *Bioorg. Med. Chem. Lett.* **2012**, *22* (4), 1793–1796.

(23) Lu, J.; Qian, Y.; Altieri, M.; Dong, H.; Wang, J.; Raina, K.; Hines, J.; Winkler, J. D.; Crew, A. P.; Coleman, K.; Crews, C. M. Hijacking the E3 Ubiquitin Ligase Cereblon to Efficiently Target BRD4. *Chem. Biol.* **2015**, *22* (6), 755–763.

(24) Bondeson, D. P.; Smith, B. E.; Burslem, G. M.; Buhimschi, A. D.; Hines, J.; Jaime-Figueroa, S.; Wang, J.; Hamman, B. D.; Ishchenko, A.; Crews, C. M. Lessons in PROTAC Design from Selective Degradation with a Promiscuous Warhead. *Cell Chem. Biol.* **2018**, *25* (1), 78–87.

(25) Zhou, B.; Hu, J.; Xu, F.; Chen, Z.; Bai, L.; Fernandez-Salas, E.; Lin, M.; Liu, L.; Yang, C. Y.; Zhao, Y.; McEachern, D.; Przybranowski, S.; Wen, B.; Sun, D.; Wang, S. Discovery of a Small-Molecule Degrader of Bromodomain and Extra-Terminal (BET) Proteins with Picomolar Cellular Potencies and Capable of Achieving Tumor Regression. *J. Med. Chem.* **2018**, *61* (2), 462–481.

(26) Nabet, B.; Roberts, J. M.; Buckley, D. L.; Paulk, J.; Dastjerdi, S.; Yang, A.; Leggett, A. L.; Erb, M. A.; Lawlor, M. A.; Souza, A.; Scott, T. G.; Vittori, S.; Perry, J. A.; Qi, J.; Winter, G. E.; Wong, K.-K.; Gray, N. S.; Bradner, J. E. The DTAG System for Immediate and Target-Specific Protein Degradation. *Nat. Chem. Biol.* **2018**, *14* (5), 431–441.

(27) Schiedel, M.; Herp, D.; Hammelmann, S.; Swyter, S.; Lehotzky, A.; Robaa, D.; Oláh, J.; Ovádi, J.; Sippl, W.; Jung, M. Chemically Induced Degradation of Sirtuin 2 (Sirt2) by a Proteolysis Targeting Chimera (PROTAC) Based on Sirtuin Rearranging Ligands (SirReals). *J. Med. Chem.* **2018**, *61* (2), 482–491.

(28) Lai, A. C.; Toure, M.; Hellerschmied, D.; Salami, J.; Jaime-Figueroa, S.; Ko, E.; Hines, J.; Crews, C. M. Modular PROTAC Design for the Degradation of Oncogenic BCR-ABL. *Angew. Chem. Int. Ed.* **2016**, *55* (2), 807–810.

(29) Burslem, G. M.; Smith, B. E.; Lai, A. C.; Jaime-Figueroa, S.; McQuaid, D. C.; Bondeson, D. P.; Toure, M.; Dong, H.; Qian, Y.; Wang, J.; Crew, A. P.; Hines, J.; Crews, C. M. The Advantages of Targeted Protein Degradation Over Inhibition: An RTK Case Study. *Cell Chem. Biol.* **2018**, *25* (1), 67–77.

(30) Li, Y.; Yang, J.; Aguilar, A.; McEachern, D.; Przybranowski, S.; Liu, L.; Yang, C.-Y.; Wang, M.; Han, X.; Wang, S. Discovery of MD-224 as a First-in-Class, Highly Potent, and Efficacious Proteolysis Targeting Chimera Murine Double Minute 2 Degrader Capable of Achieving Complete and Durable Tumor Regression. *J. Med. Chem.* **2019**, *62* (2), 448–466.

(31) Qin, C.; Hu, Y.; Zhou, B.; Fernandez-Salas, E.; Yang, C.-Y.; Liu, L.; McEachern, D.; Przybranowski, S.; Wang, M.; Stuckey, J.; Meagher, J.; Bai, L.; Chen, Z.; Lin, M.; Yang, J.; Ziazadeh, D. N.; Xu, F.; Hu, J.; Xiang, W.; Huang, L.; Li, S.; Wen, B.; Sun, D.; Wang, S. Discovery of QCA570 as an Exceptionally Potent and Efficacious Proteolysis Targeting Chimera (PROTAC) Degrader of the Bromodomain and Extra-Terminal (BET) Proteins Capable of Inducing Complete and Durable Tumor Regression. *J. Med. Chem.* **2018**, *61* (15), 6685–6704.

(32) Winter, G. E.; Buckley, D. L.; Paulk, J.; Roberts, J. M.; Souza, A.; Dhe-Paganon, S.; Bradner, J. E. Phthalimide Conjugation as a Strategy for in Vivo Target Protein Degradation. *Science* **2015**, *348* (6241), 1376–1381.

(33) Bassi, Z. I.; Fillmore, M. C.; Miah, A. H.; Chapman, T. D.; Maller, C.; Roberts, E. J.; Davis, L. C.; Lewis, D. E.; Galwey, N. W.; Waddington, K. E.; Parravicini, V.; Macmillan-Jones, A. L.; Gongora, C.; Humphreys, P. G.; Churcher, I.; Prinjha, R. K.; Tough, D. F. Modulating PCAF/GCN5 Immune Cell Function through a PROTAC Approach. *ACS Chem. Biol.* **2018**, *13* (10), 2862–2867.

(34) Yang, K.; Song, Y.; Xie, H.; Wu, H.; Wu, Y.-T.; Leisten, E. D.; Tang, W. Development of the First Small Molecule Histone Deacetylase 6 (HDAC6) Degraders. *Bioorg. Med. Chem. Lett.* **2018**, *28* (14), 2493–2497.

(35) Tang, W.; Luo, T.; Greenberg, E. F.; Bradner, J. E.; Schreiber, S. L. Discovery of Histone Deacetylase 8 Selective Inhibitors. *Bioorg. Med. Chem. Lett.* **2011**, *21* (9), 2601–2605.

(36) Jaskula-Sztul, R.; Eide, J.; Tesfazghi, S.; Dammalapati, A.; Harrison, A. D.; Yu, X.-M.; Scheinebeck, C.; Winston-McPherson, G.; Kupcho, K. R.; Robers, M. B.; Hundal, A. K.; Tang, W.; Chen, H. Tumor-Suppressor Role of Notch3 in Medullary Thyroid Carcinoma Revealed by Genetic and Pharmacological Induction. *Mol. Cancer Ther.* **2015**, *14* (2), 499–512.

(37) Jang, S.; Yu, X. M.; Odorico, S.; Clark, M.; Jaskula-Sztul, R.; Schienebeck, C. M.; Kupcho, K. R.; Harrison, A. D.; Winston-Mcpherson, G. N.; Tang, W.; Chen, H. Novel Analogs Targeting Histone Deacetylase Suppress Aggressive Thyroid Cancer Cell Growth and Induce Re-Differentiation. *Cancer Gene Ther.* **2015**, *22* (8), 410–416.

(38) Vögerl, K.; Ong, N.; Senger, J.; Herp, D.; Schmidtkunz, K.; Marek, M.; Müller, M.; Bartel, K.; Shaik, T. B.; Porter, N. J.; Robaa, D.; Christianson, D. W.; Romier, C.; Sippl, W.; Jung, M.; Bracher, F. Synthesis and Biological Investigation of Phenothiazine-Based Benzhydroxamic Acids as Selective Histone Deacetylase 6 Inhibitors. *J. Med. Chem.* **2019**, *62* (3), 1138–1166.

(39) Yu, C.-W.; Hung, P.-Y.; Yang, H.-T.; Ho, Y.-H.; Lai, H.-Y.; Cheng, Y.-S.; Chern, J.-W. Quinazolin-2,4-Dione-Based Hydroxamic Acids as Selective Histone Deacetylase-6 Inhibitors for Treatment of Non-Small Cell Lung Cancer. *J. Med. Chem.* **2019**, *62* (2), 857–874.

(40) Sellmer, A.; Stangl, H.; Beyer, M.; Grünstein, E.; Leonhardt, M.; Pongratz, H.; Eichhorn, E.; Elz, S.; Striegl, B.; Jenei-Lanzl, Z.; Dove, S.; Straub, R. H.; Krämer, O. H.; Mahboobi, S. Marbostat-100 Defines a New Class of Potent and Selective Antiinflammatory and Antirheumatic Histone Deacetylase 6 Inhibitors. *J. Med. Chem.* **2018**, *61* (8), 3454–3477.

(41) Ferreira de Freitas, R.; Harding, R. J.; Franzoni, I.; Ravichandran, M.; Mann, M. K.; Ouyang, H.; Lautens, M.; Santhakumar, V.; Arrowsmith, C. H.; Schapira, M. Identification and Structure–Activity Relationship of HDAC6 Zinc-Finger Ubiquitin Binding Domain Inhibitors. *J. Med. Chem.* **2018**, *61* (10), 4517–4527.

(42) Liu, J.-R.; Yu, C.-W.; Hung, P.-Y.; Hsin, L.-W.; Chern, J.-W. High-Selective HDAC6 Inhibitor Promotes HDAC6 Degradation Following Autophagy Modulation and Enhanced Antitumor Immunity in Glioblastoma. *Biochem. Pharmacol.* **2019**, *163*, 458–471.

(43) Lee, H.-Y.; Fan, S.-J.; Huang, F.-I.; Chao, H.-Y.; Hsu, K.-C.; Lin, T. E.; Yeh, T.-K.; Lai, M.-J.; Li, Y.-H.; Huang, H.-L.; Yang, C.-R.; Liou, J.-P. 5-Aroylindoles Act as Selective

Histone Deacetylase 6 Inhibitors Ameliorating Alzheimer's Disease Phenotypes. *J. Med. Chem.* **2018**, *61* (16), 7087–7102.

(44) Lee, H.-Y.; Nepali, K.; Huang, F.-I.; Chang, C.-Y.; Lai, M.-J.; Li, Y.-H.; Huang, H.-L.; Yang, C.-R.; Liou, J.-P. (N -Hydroxycarbonylbenylamino)Quinolines as Selective Histone Deacetylase 6 Inhibitors Suppress Growth of Multiple Myeloma in Vitro and in Vivo. *J. Med. Chem.* **2018**, *61* (3), 905–917.

(45) Bergman, J. A.; Woan, K.; Perez-Villarroel, P.; Villagra, A.; Sotomayor, E. M.; Kozikowski, A. P. Selective Histone Deacetylase 6 Inhibitors Bearing Substituted Urea Linkers Inhibit Melanoma Cell Growth. *J. Med. Chem.* **2012**, *55* (22), 9891–9899.

(46) An, Z.; Lv, W.; Su, S.; Wu, W.; Rao, Y. Developing Potent PROTACs Tools for Selective Degradation of HDAC6 Protein. *Protein Cell*. *in press*. DOI: 10.1007/s13238-018-0602-z.

(47) Papadas, A.; Asimakopoulos, F. Mechanisms of Resistance in Multiple Myeloma. In *M. Mandala, E. Romano (eds.), Mechanisms of Drug Resistance in Cancer Therapy, Handbook of Experimental Pharmacology*. Springer, **2017**, 249, 251–288.

(48) Niesvizky, R.; Richardson, P. G.; Yee, A. J.; Nooka, A. K.; Raab, M. S.; Shain, K. H.; Gabrail, N. Y.; Matous, J.; Agarwal, A. B.; Hoffman, J.; Madan, S.; Pagel, J. M.; San Miguel, J.; Moreau, P.; Mateos, M.-V.; Facon, T.; Tamang, D.; Jones, S. S.; Markelewicz, R. J.; Wheeler, C.; Trede, N. S.; Raje, N.; Terpos, E.; Bensinger, W. I. Selective HDAC6 Inhibitor ACY-241, an Oral Tablet, Combined with Pomalidomide and Dexamethasone: Safety and Efficacy of Escalation and Expansion Cohorts in Patients with Relapsed or Relapsed-and-Refractory Multiple Myeloma (ACE-MM-200 Study). *Blood* **2016**, *128* (22), 3307.

(49) Santo, L.; Hideshima, T.; Kung, A. L.; Tseng, J.-C.; Tamang, D.; Yang, M.; Jarpe, M.; van Duzer, J. H.; Mazitschek, R.; Ogier, W. C.; Cirstea, D.; Rodig, S.; Eda, H.; Scullen, T.; Canavese, M.; Bradner, J.; Anderson, K. C.; Jones, S. S.; Raje, N. Preclinical Activity, Pharmacodynamic, and Pharmacokinetic Properties of a Selective HDAC6 Inhibitor, ACY-1215, in Combination with Bortezomib in Multiple Myeloma. *Blood* **2012**, *119* (11), 2579–2589.

(50) Hideshima, T.; Cottini, F.; Ohguchi, H.; Jakubikova, J.; Gorgun, G.; Mimura, N.; Tai, Y.-T.; Munshi, N. C.; Richardson, P. G.; Anderson, K. C. Rational Combination Treatment with Histone Deacetylase Inhibitors and Immunomodulatory Drugs in Multiple Myeloma. *Blood Cancer J.* **2015**, *5* (5), 312.

(51) Ray, A.; Das, D. S.; Song, Y.; Hideshima, T.; Tai, Y.; Chauhan, D.; Anderson, K. C. Combination of a Novel HDAC6 Inhibitor ACY-241 and Anti-PD-L1 Antibody Enhances Anti-Tumor Immunity and Cytotoxicity in Multiple Myeloma. *Leukemia* **2018**, *32* (3), 843–846.

(52) Kronke, J.; Udeshi, N. D.; Narla, A.; Grauman, P.; Hurst, S. N.; McConkey, M.; Svinkina, T.; Heckl, D.; Comer, E.; Li, X.; Ciarlo, C.; Hartman, E.; Munshi, N.; Schenone, M.; Schreiber, S. L.; Carr, S. A.; Ebert, B. L. Lenalidomide Causes Selective Degradation of IKZF1 and IKZF3 in Multiple Myeloma Cells. *Science* **2014**, *343* (6168), 301–305.

(53) Fischer, E. S.; Böhm, K.; Lydeard, J. R.; Yang, H.; Stadler, M. B.; Cavadini, S.; Nagel, J.; Serluca, F.; Acker, V.; Lingaraju, G. M.; Tichkule, R. B.; Schebesta, M.; Forrester, W. C.; Schirle, M.; Hassiepen, U.; Ottl, J.; Hild, M.; Beckwith, R. E. J.; Harper, J. W.; Jenkins, J. L.; Thomä, N. H. Structure of the DDB1–CRBN E3 Ubiquitin Ligase in Complex with

Thalidomide. *Nature* **2014**, *512* (7512), 49–53.

(54) Lu, G.; Middleton, R. E.; Sun, H.; Naniong, M.; Ott, C. J.; Mitsiades, C. S.; Wong, K.-K.; Bradner, J. E.; Kaelin, W. G. The Myeloma Drug Lenalidomide Promotes the Cereblon-Dependent Destruction of Ikaros Proteins. *Science* **2014**, *343* (6168), 305–309.

(55) Matyskiela, M. E.; Lu, G.; Ito, T.; Pagarigan, B.; Lu, C.-C.; Miller, K.; Fang, W.; Wang, N.-Y.; Nguyen, D.; Houston, J.; Carmel, G.; Tran, T.; Riley, M.; Nosaka, L.; Lander, G. C.; Gaidarova, S.; Xu, S.; Ruchelman, A. L.; Handa, H.; Carmichael, J.; Daniel, T. O.; Cathers, B. E.; Lopez-Girona, A.; Chamberlain, P. P. A Novel Cereblon Modulator Recruits GSPT1 to the CRL4CRBN Ubiquitin Ligase. *Nature* **2016**, *535* (7611), 252–257.

(56) Zorba, A.; Nguyen, C.; Xu, Y.; Starr, J.; Borzilleri, K.; Smith, J.; Zhu, H.; Farley, K. A.; Ding, W.; Schiemer, J.; Feng, X.; Chang, J. S.; Uccello, D. P.; Young, J. A.; Garcia-Irrizary, C. N.; Czabaniuk, L.; Schuff, B.; Oliver, R.; Montgomery, J.; Hayward, M. M.; Coe, J.; Chen, J.; Niosi, M.; Luthra, S.; Shah, J. C.; El-Kattan, A.; Qiu, X.; West, G. M.; Noe, M. C.; Shanmugasundaram, V.; Gilbert, A. M.; Brown, M. F.; Calabrese, M. F. Delineating the Role of Cooperativity in the Design of Potent PROTACs for BTK. *Proc. Natl. Acad. Sci.* **2018**, *115* (31), 7285–7292.

(57) Nowak, R. P.; DeAngelo, S. L.; Buckley, D.; He, Z.; Donovan, K. A.; An, J.; Safaee, N.; Jedrychowski, M. P.; Ponthier, C. M.; Ishoey, M.; Zhang, T.; Mancias, J. D.; Gray, N. S.; Bradner, J. E.; Fischer, E. S. Plasticity in Binding Confers Selectivity in Ligand-Induced Protein Degradation. *Nat. Chem. Biol.* **2018**, *14* (7), 706–714.

(58) Wang, J.; Liang, Y.-L.; Qu, J. Boiling Water-Catalyzed Neutral and Selective N-Boc Deprotection. *Chem. Commun.* **2009**, 5144.

(59) Evans, R. A. The Rise of Azide–Alkyne 1,3-Dipolar "Click" Cycloaddition and Its Application to Polymer Science and Surface Modification. *Aust. J. Chem.* **2007**, *60* (6), 384–395.

(60) Chamberlain, P. P.; Lopez-Girona, A.; Miller, K.; Carmel, G.; Pagarigan, B.; Chie-Leon, B.; Rychak, E.; Corral, L. G.; Ren, Y. J.; Wang, M.; Riley, M.; Delker, S. L.; Ito, T.; Ando, H.; Mori, T.; Hirano, Y.; Handa, H.; Hakoshima, T.; Daniel, T. O.; Cathers, B. E. Structure of the Human Cereblon-DDB1-Lenalidomide Complex Reveals Basis for Responsiveness to Thalidomide Analogs. *Nat. Struct. Mol. Biol.* **2014**, *21* (9), 803–809.

(61) Miyake, Y.; Keusch, J. J.; Wang, L.; Saito, M.; Hess, D.; Wang, X.; Melancon, B. J.; Helquist, P.; Gut, H.; Matthias, P. Structural Insights into HDAC6 Tubulin Deacetylation and Its Selective Inhibition. *Nat. Chem. Biol.* **2016**, *12* (9), 748–754.

(62) Finnin, M. S.; Donigian, J. R.; Cohen, A.; Richon, V. M.; Rifkind, R. A.; Marks, P. A.; Breslow, R.; Pavletich, N. P. Structures of a Histone Deacetylase Homologue Bound to the TSA and SAHA Inhibitors. *Nature* **1999**, *401* (6749), 188–193.

(63) Douglass, E. F.; Miller, C. J.; Sparer, G.; Shapiro, H.; Spiegel, D. A. A Comprehensive Mathematical Model for Three-Body Binding Equilibria. *J. Am. Chem. Soc.* **2013**, *135* (16), 6092–6099.

(64) Soucy, T. A.; Smith, P. G.; Milhollen, M. A.; Berger, A. J.; Gavin, J. M.; Adhikari, S.; Brownell, J. E.; Burke, K. E.; Cardin, D. P.; Critchley, S.; Cullis, C. A.; Doucette, A.; Garnsey, J. J.; Gaulin, J. L.; Gershman, R. E.; Lublinsky, A. R.; McDonald, A.; Mizutani, H.; Narayanan, U.; Olhava, E. J.; Peluso, S.; Rezaei, M.; Sintchak, M. D.; Talreja, T.; Thomas, M. P.; Traore, T.; Vyskocil, S.; Weatherhead, G. S.; Yu, J.; Zhang, J.; Dick, L. R.;

Claiborne, C. F.; Rolfe, M.; Bolen, J. B.; Langston, S. P. An Inhibitor of NEDD8-Activating Enzyme as a New Approach to Treat Cancer. *Nature* **2009**, *458* (7239), 732–736.

(65) Yee, A. J.; Bensinger, W. I.; Supko, J. G.; Voorhees, P. M.; Berdeja, J. G.; Richardson, P. G.; Libby, E. N.; Wallace, E. E.; Birrer, N. E.; Burke, J. N.; Tamang, D. L.; Yang, M.; Jones, S. S.; Wheeler, C. A.; Markelewicz, R. J.; Raje, N. S. Ricolinostat plus Lenalidomide, and Dexamethasone in Relapsed or Refractory Multiple Myeloma: A Multicentre Phase 1b Trial. *Lancet Oncol.* **2016**, *17* (11), 1569–1578.

(66) Harada, T.; Hideshima, T.; Anderson, K. C. Histone Deacetylase Inhibitors in Multiple Myeloma: From Bench to Bedside. *Int. J. Hematol.* **2016**, *104* (3), 300–309.

(67) Andersen, P. L.; Vermette, P. Intracellular Insulin Quantification by Cell-ELISA. *Exp. Cell Res.* **2016**, *347* (1), 14–23.

(68) Livak, K. J.; Schmittgen, T. D. Analysis of Relative Gene Expression Data Using Real-Time Quantitative PCR and the 2 C T Method. *Methods* **2001**, *25*, 402–408.

Table of contents graphic